IEEE Access
Multidisciplinary ⋮ Rapid Review ⋮ Open Access Journal

Received 10 June 2022, accepted 28 July 2022, date of publication 8 August 2022, date of current version 17 August 2022.

Digital Object Identifier 10.1109/ACCESS.2022.3197223

RESEARCH ARTICLE

Locational Marginal Price Decomposition Using a Fully Distributed Slack Bus Model

FELIPE O. S. SARAIVA, (Member, IEEE), AND V. LEONARDO PAUCAR, (Senior Member, IEEE)
Department of Electrical Engineering, Federal University of Maranhão, São Luís 65085-580, Brazil

Corresponding author: Felipe O. S. Saraiva (felipe_saraiva@ieee.org)

This work was supported in part by the Coordenação de Aperfeiçoamento de Pessoal de Nível Superior—Brasil (CAPES)—Finance Code 001 under Grant 88887.626552/2021-00.

ABSTRACT The implementation of risk hedging instruments against the inherent volatile nature of locational marginal prices (LMPs) requires the decomposition of such economic signals into specific components. These components are dependent on the active energy reference selection in optimal power flow (OPF) models that govern the LMP decomposition. Active power distributed slack bus models are commonly used to set the active energy reference in LMP decomposition frameworks to satisfy the financial interests of electricity market participants more equitably. However, in recent years, some important energy-related organizations have shown interest in incorporating reactive power into market-oriented OPF models. This scenario highlights the need for research efforts focused on the formulation of distributed slack bus models that address active and reactive powers. In this context, this paper proposes an LMP decomposition model based on an OPF framework with a fully distributed slack bus formulation. The harmful financial impacts of conventional reactive energy reference specification strategies in the calculation of LMP components are explained from the perspective of market participants. In the proposed decomposition model, to overcome such impacts, active and reactive power mismatches are compensated through the conventional active power distributed slack bus and the proposed reactive power distributed slack bus, respectively. Thus, the double selection of energy reference conceives a new source of negotiation between market participants in the formulation of risk hedging instruments. Numerical simulations on the IEEE 30-bus test system show that differences between LMP congestion components can change by 8.1300% for feasible variations in the reactive energy reference specification.

INDEX TERMS Electricity markets, LMP decomposition, locational marginal price (LMP), optimal power flow (OPF), reactive energy reference, reactive power distributed slack bus.

NOMENCLATURE

$\mathrm{F}(\cdot)$	Total operating cost function.
$\boldsymbol{I}_i$	$i \times i$ identity matrix.
n, n_{pv}, n_b, n_g	Total number of buses, PV buses, branches, and generators.
$\boldsymbol{p}, \boldsymbol{q}$	Vectors of net active and reactive power injections at all buses, i.e., $\boldsymbol{p} = \boldsymbol{p}_g - \boldsymbol{p}_d$ and $\boldsymbol{q} = \boldsymbol{q}_g - \boldsymbol{q}_d$.
$\boldsymbol{p}_d, \boldsymbol{q}_d$	Vectors of active and reactive power loads at all buses.
p_{ds}, q_{ds}	Active and reactive power injections at the corresponding distributed slack buses.
$\boldsymbol{p}_f, \boldsymbol{q}_f$	Vectors of active and reactive power flow functions at all buses.
$\boldsymbol{p}_g, \boldsymbol{q}_g$	Vectors of active and reactive power injections at all buses.
$\boldsymbol{s}_{fl}$	Vector of apparent power flows at all branches.
$\boldsymbol{\alpha}, \boldsymbol{\beta}$	Vectors of active and reactive power participation factors.
$\overline{\boldsymbol{\eta}}_p, \underline{\boldsymbol{\eta}}_p, \overline{\boldsymbol{\eta}}_q, \underline{\boldsymbol{\eta}}_q$	Vectors of Lagrange multipliers.
$\boldsymbol{\lambda}_p, \boldsymbol{\lambda}_q$	Vectors of active and reactive power LMPs at all buses.

The associate editor coordinating the review of this manuscript and approving it for publication was Behnam Mohammadi-Ivatloo.

$\lambda_{p_{ds}}, \lambda_{q_{ds}}$	Active and reactive power LMPs at the corresponding distributed slack buses.
$\boldsymbol{\lambda}_p^e, \boldsymbol{\lambda}_p^{pl}, \boldsymbol{\lambda}_p^c$	Vectors of active energy, active power loss, and congestion components of active power LMPs.
$\boldsymbol{\lambda}_p^{ql}, \boldsymbol{\lambda}_p^x$	Vectors of reactive power loss and state constraint components of active power LMPs.
$\boldsymbol{\mu}, \overline{\boldsymbol{\varphi}}, \underline{\boldsymbol{\varphi}}$	Vectors of Lagrange multipliers explicitly used in the calculation of LMP components.
$\mathbf{0}_i, \mathbf{1}_i$	$i \times 1$ vectors fully composed of zeros and ones.

I. INTRODUCTION

A. BACKGROUND AND MOTIVATION

Over the last few decades, aiming to propagate economic efficiency through the different instances of the electric power industry, locational marginal prices (LMPs) have emerged as the basis of modern electricity market designs. The conceptual and mathematical genesis of LMPs comes from the propositions in [1], which provided short-term financial directives for promoting economic efficiency in the use of electric power system (EPS) resources. This locational approach concerning electricity pricing was expanded in [2] to encompass practical applications. However, owing to the unavoidable uncertainties inherent in EPS operations, LMPs typically exhibit significant spatiotemporal volatility. This monetary variability poses a substantial risk to the financial goals of many electricity market participants. Therefore, risk hedging instruments need to be adopted to mitigate the harmful impacts associated with the aforementioned economic risk. The formulation of risk hedging instruments is based on specific marginal components computed using appropriate LMP decomposition models. The most widespread and consolidated risk hedging instruments in the current electricity market scenario governed by LMPs are the financial transmission rights (FTRs), originally proposed in [2] and [3]. FTRs are hedging tools used to mitigate the financial risks related to transmission congestion via a payment scheme based on LMP congestion components.

A significant portion of the optimal power flow (OPF) models that govern the current LMP decomposition frameworks use distributed slack strategies to offset mismatches between active power generation, demand, and losses. However, in the context of power flow formulations typically included in OPF constraints, the compensation schemes for dealing with mismatches between reactive power generation, load, and losses have remained essentially the same throughout the literature on LMP decomposition. Such reactive power compensation approaches are generally based on two modelling approaches. The first considers that reactive power counterbalances are integrally performed on a single energy reference bus, as assumed in [4]. This single energy reference bus is simultaneously an active energy reference bus and a reactive energy reference bus. The second approach assumes a set of simplifying conditions that makes it possible to disregard the variables associated with reactive power. This methodology corresponds to that adopted in most proposals presented in the LMP decomposition literature, as considered in [5], [6], [7], and [8]. In this work, power compensations always refer to those used in the post-optimization energy reference (distributed slack) specifications of OPF models that govern LMP decomposition schemes. In simplified LMP decomposition models that neglect the constraints related to reactive power variables, the reactive power loss components of the LMPs are not computed. On the other hand, in LMP decomposition approaches in which reactive power offsets are performed on a single reactive energy reference bus, the reactive power loss components of LMPs may or may not be calculated depending on the OPF framework constraints. If computed, the reactive power loss component of the LMP associated with a given bus represents the marginal cost of reactive power losses when the source of the active power increment is located at this bus, and reactive power compensation is performed on the single energy reference bus. Therefore, using this class of reactive power compensation strategies may adversely affect the financial goals of certain electricity market participants. This harmful impact is similar to that discussed in [5] regarding the active power loss components of LMPs derived from decomposition models in which active power compensation is performed on a single active energy reference bus.

In the context of current technical-economic practices, market settlements are usually performed by independent system operators (ISOs) based on solving direct current optimal power flow (DCOPF) models. Generation scheduling and electricity price calculations usually satisfy the time requirements for electricity market operations due to solution approaches typically applied in DCOPF frameworks. However, the use of DCOPF models implies many operational and financial adversities highlighted in current market experiences and research findings. The modelling oversimplification used in the DCOPF formulations requires constant ISO intervention in real-time, intraday, and day-ahead markets [9]. Furthermore, the mismatch between the LMPs calculated based on DCOPF approaches and the true EPS marginal costs requires the implementation of uplift payment schemes [9]. LMP derivations are not fully available in ISO manuals and tariff reports [10], which adds a lack of transparency to an environment governed by prices that often do not correspond to real-world market operations. In the AC feasibility assurance process associated with DCOPF frameworks, ISOs usually employ nomogram constraints to represent the voltage limits and reactive power requirements [11]. Thus, different model specifications that represent the same EPS constraints can result in different spatiotemporal LMP patterns [11]. For example, significantly different LMP profiles resulting from the imposition of different nomogram constraints to represent the same voltage constraints were shown in [12]. In the context of practical applications, the Midwest ISO (MISO)

has observed that nomograms do not perform satisfactorily under voltage constraints [11]. California ISO (CAISO) has reported that difficulties in meeting reactive power demand have been the main source of voltage instability, a problem that has worsened with increasing active power transfer in the electrical grid [11], [13]. Given these shortcomings, a report produced by the Federal Energy Regulatory Commission (FERC) [14] shows that there is significant interest in employing alternating current optimal power flow (ACOPF) models in real-world applications. The study carried out in [15] and supported by the United States Department of Energy (DOE) recommends intensifying efforts to improve nonlinear, non-convex optimization algorithms dedicated to solving ACOPF problems for market applications. A DOE report addressed to the United States Congress [16] pointed out the need for more accurate investigations into the technical quality of algorithms, software, data, and hypotheses considered in current economic dispatch practices, which could improve the reliability and viability of the national energy supply.

Thus, there are two main reasons that justify the proposition of a new reactive power compensation scheme to be incorporated into OPF frameworks that govern LMP decomposition models. The first corresponds to the aforementioned possible harmful impacts on the financial interests of market participants concerning the use of traditional reactive power compensation schemes in conventional LMP decomposition models. The second refers to the growing interest of important state entities, the research community, and relevant market participants in the incorporation of reactive power into dispatch models that govern the market settlement process.

B. LITERATURE REVIEW

An enlightening investigation of LMP decomposition into three components was conducted in [17]. An LMP decomposition model based on a decoupled OPF formulation consisting of independent active and reactive power optimization instances was proposed in [18]. In [19], an approach for disaggregating active and reactive power spot prices into two components was presented. In such a scheme, one component is related to operational constraints and the other simultaneously reflects generation and losses. In the pricing methodology proposed in [4], spot prices are decomposed into four components: system marginal cost, security cost, loss compensation cost, and loss cost associated with the coupling between active and reactive powers. A nodal price decomposition scheme was conceived in [20], in which prices were fragmented into a wide range of components associated with various descriptive aspects of an EPS. In [21], a strategy for measuring the contributions of different electricity market participants to the composition of congestion components of nodal prices was introduced.

An LMP decomposition scheme based on loss allocation via a distributed slack framework constituting a DCOPF was described in [22]. In the LMP decomposition approach proposed in [5], inadequate market conditions concerning OPF single slack bus models are overcome through a distributed slack bus formulation. To overcome the reference dependency, an energy reference bus independent LMP decomposition model was proposed in [23]. A methodology for accurately measuring market participant impacts in computing nodal price loss components during congestion scenarios was presented in [24]. A DCOPF framework governed by a fictitious nodal demand model was proposed in [25] for the LMP calculation and decomposition. A fourth LMP component, called the future limit risk price, is derived in the continuous LMP model described in [26]. The broad formulation conceived in [6] encompasses different LMP decomposition models and highlights the leading role of marginal generator buses. In [27], a decomposition model that measures the impact of various factors on the expected value and standard deviation of LMPs was presented. A conciliatory methodology for resolving disputes concerning the energy reference specification to provide an adequate LMP decomposition policy for FTR implementation was presented in [7]. In [28], the formulation of a new LMP component, called the marginal security component, was proposed to quantify the implications of the generator contingency constraints. An LMP decomposition scheme that measures the impact of binding transmission and voltage constraints was formulated in [29]. A decomposition methodology anchored in the structural fragmentation of LMPs and power generation for the investigation of collusion in electricity markets was conceived in [30]. To examine the impacts of renewable generation on LMPs, a decomposition model was introduced in [31] to assess the effects of the strategic behavior of generation companies and the EPS structure on LMPs. More recently, the market modelling merits provided by LMPs have penetrated the scope of distribution systems in the form of distribution LMPs (DLMPs). DLMP decomposition frameworks were proposed in [32], [33], [34], and [35].

C. CONTRIBUTIONS

This paper proposes an LMP decomposition model derived from an OPF formulation that, in addition to incorporating the conventional active power distributed slack strategy, encompasses a new reactive power distributed slack scheme. The main contributions of this work can be summarized as follows:

1) The impact of the proposed reactive power distributed compensation framework on the active power-based market settlement process is demonstrated. Such a decomposition approach shows that the effects of energy reference selection on the computation of LMP components are not restricted to the active energy reference specification conventionally employed in LMP decomposition strategies but also encompasses reactive energy reference selection.
2) Since FTRs are the risk hedging instruments mostly used in LMP-based markets, special attention is given to the impacts of the proposed decomposition framework on the financial magnitude of the LMP congestion

components. In the proposed fully distributed slack model, the computation of the LMP congestion components now depends on the specification of active and reactive energy references, which allows FTRs to be settled under terms that more accurately reflect the interests of market participants.

3) The independence of LMP decomposition approaches with respect to the adoption of different power sensitivity classes is demonstrated, whereas the reactive power distributed compensation scheme used in conventional power flow formulations is proven to be inadequate for such decomposition models.

D. PAPER ORGANIZATION

The remainder of this paper is organized as follows. In Section II, optimality-based formulations and some important caveats of conventional LMP decomposition models are presented. The proposed LMP decomposition framework, based on an OPF model governed by a fully distributed compensation scheme, is derived in Section III. The market impacts of the proposed decomposition scheme on the financial breadth associated with hedging mechanisms, such as FTRs, are evaluated through numerical simulations presented in Section IV. The contributions of this paper are summarized in Section V.

II. CORNERSTONE AND REMARKS OF LMP DECOMPOSITION MODELS

In this section, the LMP decomposition model governed by the conventional active power distributed slack scheme is formulated and discussed. Additionally, alternative decomposition approaches are presented to highlight some caveats concerning the LMP breakdown.

A. LMP DECOMPOSITION MODEL BASED ON A CONVENTIONAL DISTRIBUTED SLACK FRAMEWORK

Before proceeding, it is important to clarify that, as highlighted in [23], the concept of a conventional slack bus is different from the definition of an active power distributed slack bus and an active energy reference bus. In the context of traditional power flow formulations, it is well known that a slack bus defines the angular reference of an EPS and has a fixed voltage magnitude and angle. In optimization environments, such as those in OPF frameworks, the specification of the slack bus represents an excessive requirement, as it can overly constrain optimization problems [36]. In power flow formulations, an active power distributed slack bus is a fictitious bus whose active power injection is distributed across all buses based on preset participation factors. The active power distributed slack bus is used to balance the mismatch between active power generation, demand, and losses. However, in the context of OPF frameworks, the use of active power distributed slack bus makes sense only for post-optimization LMP decomposition purposes. Therefore, in this work, OPF models governing LMP decomposition schemes always refer to models used in the post-optimization mathematical derivation of LMP components. The active power distributed slack bus defines the active energy reference bus. Thus, in OPF approaches, active power distributed slack and active energy reference buses can be mentioned interchangeably. The slack bus can coincide with the active power distributed slack bus (active energy reference bus), although this is not common practice [23]. This coincidence is verified when the participation factors of all EPS buses in an active power distributed slack bus approach are zero, except that related to the slack bus, which is equal to one.

In the OPF frameworks that govern most LMP decomposition approaches, power mismatch compensation methodologies are based either on traditional power flow equations or on the incorporation of distributed slack bus to handle only active power in the context of power flow formulations. Here, the conventional LMP decomposition approach is based on an OPF formulation with an active power distributed slack bus model. This OPF formulation aims to minimize the total operating cost without violating a predefined set of EPS constraints. The main challenge associated with modelling the decomposition approach based on the present OPF framework is the implementation of the post-optimization sensitivity vectors used in the LMP decomposition equations. Following the assumptions made in [5], [6], and [7], the current OPF model considers that there is sufficient reactive power availability to maintain EPS bus voltage magnitudes of one per unit. Thus, the OPF framework is defined as:

$$\min \ \mathrm{F}\left(\boldsymbol{p}_{gb}\right) = \sum_{i=1}^{n_g} \mathrm{C}_i\left(p_{gb,i}\right) \tag{1}$$

$$\text{s.t. } p_{ds} = 0 \tag{2}$$

$$-\boldsymbol{p}_g - \boldsymbol{\alpha} p_{ds} + \boldsymbol{p}_d + \boldsymbol{p}_f = \mathbf{0}_n \tag{3}$$

$$\boldsymbol{s}_{fl} - \boldsymbol{s}_{fl}^{max} \leq \mathbf{0}_{2n_b} \tag{4}$$

$$\boldsymbol{p}_{gb} - \boldsymbol{p}_{gb}^{max} \leq \mathbf{0}_{n_g} \tag{5}$$

$$-\boldsymbol{p}_{gb} + \boldsymbol{p}_{gb}^{min} \leq \mathbf{0}_{n_g} \tag{6}$$

where $\mathrm{C}_i\left(p_{gb,i}\right)$ denotes the bid function submitted by the *ith* generator. The superscripts $(\cdot)^{max}$ and $(\cdot)^{min}$ represent the upper and lower limits of the quantities associated with these notations, respectively. The vector $\boldsymbol{p}_{gb}$ is formed by the active power injections at generation buses, and is given by:

$$\boldsymbol{p}_{gb} = \boldsymbol{A}_g \boldsymbol{p}_g \tag{7}$$

where $\boldsymbol{A}_g$ is an $n_g \times n$ matrix whose generic element $A_{g,ij}$ is equal to one if the *ith* generator is connected to the *jth* bus or is equal to zero otherwise. The scalar $p_{gb,i}$ is the *ith* element of the vector $\boldsymbol{p}_{gb}$. In the present OPF approach, the active power injection in the active power distributed slack bus must be zero, which is represented by constraint (2). Equation (3) encompasses the active power balance constraints for all buses. Inequality (4) is composed of transmission capacity constraints. To make the current model compatible with the OPF formulations presented later, the transmission capacity constraints in (4) are expressed in terms of apparent power

flows. Inequalities (5) and (6) represent the upper and lower limits of active power generation, respectively.

The Lagrange function of the OPF problem formulated in (1)–(6) can be written as follows:

$$\begin{aligned} \mathrm{L} = {} & \mathrm{F}\left(\boldsymbol{p}_{gb}\right) + p_{ds}\lambda_{p_{ds}} + \left[\boldsymbol{s}_{fl} - \boldsymbol{s}_{fl}^{max}\right]^T \boldsymbol{\mu} \\ & + \left[-\boldsymbol{p}_g - \boldsymbol{\alpha} p_{ds} + \boldsymbol{p}_d + \boldsymbol{p}_f\right]^T \boldsymbol{\lambda}_p \\ & + \left[\boldsymbol{p}_{gb} - \boldsymbol{p}_{gb}^{max}\right]^T \overline{\boldsymbol{\eta}}_p + \left[-\boldsymbol{p}_{gb} + \boldsymbol{p}_{gb}^{min}\right]^T \underline{\boldsymbol{\eta}}_p. \end{aligned} \tag{8}$$

The Karush–Kuhn–Tucker (KKT) necessary conditions for optimality of the OPF solution are derived as:

$$\frac{\partial \mathrm{L}}{\partial \boldsymbol{p}_{gb}} = \frac{\partial \mathrm{F}}{\partial \boldsymbol{p}_{gb}} - \boldsymbol{\lambda}_{p_{gb}} + \overline{\boldsymbol{\eta}}_p - \underline{\boldsymbol{\eta}}_p = \boldsymbol{0}_{n_g} \tag{9}$$

$$\frac{\partial \mathrm{L}}{\partial \boldsymbol{\theta}} = \left(\frac{\partial \boldsymbol{p}_f}{\partial \boldsymbol{\theta}}\right)^T \boldsymbol{\lambda}_p + \left(\frac{\partial \boldsymbol{s}_{fl}}{\partial \boldsymbol{\theta}}\right)^T \boldsymbol{\mu} = \boldsymbol{0}_{n-1} \tag{10}$$

$$\frac{\partial \mathrm{L}}{\partial p_{ds}} = \lambda_{p_{ds}} - \boldsymbol{\alpha}^T \boldsymbol{\lambda}_p = 0 \tag{11}$$

where $\boldsymbol{\theta}$ is the vector containing the voltage angles at all buses except the EPS slack bus. The vector $\boldsymbol{\lambda}_{p_{gb}}$ is formed by the LMPs at the generation buses and is obtained as follows:

$$\boldsymbol{\lambda}_{p_{gb}} = \boldsymbol{A}_g \boldsymbol{\lambda}_p. \tag{12}$$

For simplicity, the complementary slackness conditions are not presented in this paper. Furthermore, in the notational definitions used in this work, LMP and active power LMP can be used interchangeably. By rearranging (10) and (11), the following equality can be obtained:

$$\begin{aligned} & \begin{bmatrix} \left(\frac{\partial \boldsymbol{p}_f}{\partial \boldsymbol{\theta}}\right)^T \boldsymbol{\lambda}_p \\ -\boldsymbol{\alpha}^T \boldsymbol{\lambda}_p \end{bmatrix} \\ & = \begin{bmatrix} -\left(\frac{\partial \boldsymbol{s}_{fl}}{\partial \boldsymbol{\theta}}\right)^T \boldsymbol{\mu} \\ -\lambda_{p_{ds}} \end{bmatrix} \\ & \Longrightarrow \begin{bmatrix} \left(\frac{\partial \boldsymbol{p}_f}{\partial \boldsymbol{\theta}}\right)^T \\ -\boldsymbol{\alpha}^T \end{bmatrix} \boldsymbol{\lambda}_p = \begin{bmatrix} -\left(\frac{\partial \boldsymbol{s}_{fl}}{\partial \boldsymbol{\theta}}\right)^T \boldsymbol{\mu} \\ -\lambda_{p_{ds}} \end{bmatrix} \\ & \Longrightarrow \boldsymbol{\lambda}_p = \left[\begin{bmatrix} \frac{\partial \boldsymbol{p}_f}{\partial \boldsymbol{\theta}} & -\boldsymbol{\alpha} \end{bmatrix}^{-1}\right]^T \begin{bmatrix} -\left(\frac{\partial \boldsymbol{s}_{fl}}{\partial \boldsymbol{\theta}}\right)^T \boldsymbol{\mu} \\ -\lambda_{p_{ds}} \end{bmatrix}. \end{aligned} \tag{13}$$

By differentiating (3) with respect to $\boldsymbol{p}$, the Jacobian matrix of the power flow equations in (3) can be derived as follows:

$$\begin{aligned} & -\frac{\partial\left(\boldsymbol{p}_g - \boldsymbol{p}_d\right)}{\partial \boldsymbol{p}} - \boldsymbol{\alpha}\left(\frac{\partial p_{ds}}{\partial \boldsymbol{p}}\right)^T + \frac{\partial \boldsymbol{p}_f}{\partial \boldsymbol{p}} = \boldsymbol{0}_{n\times n} \\ & \Longrightarrow -\frac{\partial \boldsymbol{p}}{\partial \boldsymbol{p}} - \boldsymbol{\alpha}\left(\frac{\partial p_{ds}}{\partial \boldsymbol{p}}\right)^T + \frac{\partial \boldsymbol{p}_f}{\partial \boldsymbol{\theta}}\frac{\partial \boldsymbol{\theta}}{\partial \boldsymbol{p}} = \boldsymbol{0}_{n\times n} \\ & \Longrightarrow \begin{bmatrix} \frac{\partial \boldsymbol{p}_f}{\partial \boldsymbol{\theta}} & -\boldsymbol{\alpha} \end{bmatrix} \begin{bmatrix} \frac{\partial \boldsymbol{\theta}}{\partial \boldsymbol{p}} \\ \left(\frac{\partial p_{ds}}{\partial \boldsymbol{p}}\right)^T \end{bmatrix} = \boldsymbol{I}_n \end{aligned}$$

$$\Longrightarrow \begin{bmatrix} \frac{\partial \boldsymbol{p}_f}{\partial \boldsymbol{\theta}} & -\boldsymbol{\alpha} \end{bmatrix} = \begin{bmatrix} \frac{\partial \boldsymbol{\theta}}{\partial \boldsymbol{p}} \\ \left(\frac{\partial p_{ds}}{\partial \boldsymbol{p}}\right)^T \end{bmatrix}^{-1} \tag{14}$$

where $\boldsymbol{0}_{i\times i}$ is a $i \times i$ matrix fully composed of zeros.

Now, substituting (14) into (13) gives

$$\begin{aligned} \boldsymbol{\lambda}_p &= \begin{bmatrix} \left(\frac{\partial \boldsymbol{\theta}}{\partial \boldsymbol{p}}\right)^T & \frac{\partial p_{ds}}{\partial \boldsymbol{p}} \end{bmatrix} \begin{bmatrix} -\left(\frac{\partial \boldsymbol{s}_{fl}}{\partial \boldsymbol{\theta}}\right)^T \boldsymbol{\mu} \\ -\lambda_{p_{ds}} \end{bmatrix} \\ &= -\frac{\partial p_{ds}}{\partial \boldsymbol{p}}\lambda_{p_{ds}} - \left(\frac{\partial \boldsymbol{\theta}}{\partial \boldsymbol{p}}\right)^T \left(\frac{\partial \boldsymbol{s}_{fl}}{\partial \boldsymbol{\theta}}\right)^T \boldsymbol{\mu}. \end{aligned} \tag{15}$$

The network active power losses are calculated as follows:

$$p_l = \boldsymbol{1}_n^T \boldsymbol{p} + p_{ds}. \tag{16}$$

Thus, by differentiating (16) with respect to $\boldsymbol{p}$, the vector relation containing the loss sensitivity factors is computed as follows:

$$\frac{\partial p_{ds}}{\partial \boldsymbol{p}} = -\boldsymbol{1}_n + \frac{\partial p_l}{\partial \boldsymbol{p}}. \tag{17}$$

Finally, substituting (17) into (15) results in:

$$\boldsymbol{\lambda}_p = \underbrace{\boldsymbol{1}_n \lambda_{p_{ds}}}_{\lambda_p^e} \underbrace{- \frac{\partial p_l}{\partial \boldsymbol{p}}\lambda_{p_{ds}}}_{\lambda_p^{pl}} \underbrace{- \left(\frac{\partial \boldsymbol{s}_{fl}}{\partial \boldsymbol{p}}\right)^T \boldsymbol{\mu}}_{\lambda_p^c}. \tag{18}$$

Equation (18) provides the three classical LMP components derived from the decomposition model based on the conventional distributed slack approach.

B. DECOMPOSITION APPROACH BASED ON A CENTRALIZED REACTIVE SLACK SCHEME

In this section, the impact of including a conventional reactive power mismatch compensation scheme in the context of LMP decomposition models is derived. For this purpose, in the OPF model that underpins the LMP decomposition scheme considered here, the active power counterbalance follows the strategy formulated in Section II-A and the reactive power compensation follows the scheme adopted in [4]. The inclusion of the conventional reactive power compensation approach imposes an additional modelling hurdle, as it increases the complexity of implementing the post-optimization sensitivity vectors that form the LMP decomposition equations. In this centralized reactive power compensation model, the offset of mismatches between reactive power generation, load, and losses is performed exclusively on a reactive energy reference bus. It is important to note that despite being conceptually different, slack, active energy reference, and reactive energy reference buses can alternatively coincide. For example, it is possible for the slack bus to coincide with only the active energy reference bus, only the reactive energy reference bus, both energy reference buses, or none of the energy reference buses. In this context, the OPF problem is formulated as follows:

$$\min \ \mathrm{F}\left(\boldsymbol{p}_{gb}\right) \tag{19}$$

$$\text{s.t.} \; -q_{g,r} + q_{d,r} + q_{f,r} = 0 \tag{20}$$
$$-\boldsymbol{q}_{g,\bar{r}} + \boldsymbol{q}_{d,\bar{r}} + \boldsymbol{q}_{f,\bar{r}} = \mathbf{0}_{n-1} \tag{21}$$
$$\boldsymbol{q}_{gb} - \boldsymbol{q}_{gb}^{max} \leq \mathbf{0}_{n_g} \tag{22}$$
$$-\boldsymbol{q}_{gb} + \boldsymbol{q}_{gb}^{min} \leq \mathbf{0}_{n_g} \tag{23}$$
$$\boldsymbol{x} - \boldsymbol{x}^{max} \leq \mathbf{0}_{2n-2} \tag{24}$$
$$-\boldsymbol{x} + \boldsymbol{x}^{min} \leq \mathbf{0}_{2n-2} \tag{25}$$
$$(2)\text{–}(6)$$

where $q_{g,r}$, $q_{d,r}$, and $q_{f,r}$ denote the elements associated with the reactive energy reference bus in vectors $\boldsymbol{q}_g$, $\boldsymbol{q}_d$, and $\boldsymbol{q}_f$, respectively. Similarly, $\boldsymbol{q}_{g,\bar{r}}$, $\boldsymbol{q}_{d,\bar{r}}$, and $\boldsymbol{q}_{f,\bar{r}}$ are vectors containing only the elements associated with buses that are not the reactive energy reference bus in vectors $\boldsymbol{q}_g$, $\boldsymbol{q}_d$, and $\boldsymbol{q}_f$, respectively. The vector $\boldsymbol{q}_{gb}$ is formed by reactive power injections at generation buses. Specifically, these relationships can be defined as follows:

$$\begin{bmatrix} q_{g,r} & q_{d,r} & q_{f,r} \\ \boldsymbol{q}_{g,\bar{r}} & \boldsymbol{q}_{d,\bar{r}} & \boldsymbol{q}_{f,\bar{r}} \end{bmatrix} = \begin{bmatrix} \boldsymbol{a}_r^T \\ \boldsymbol{A}_{\bar{r}} \end{bmatrix} \begin{bmatrix} \boldsymbol{q}_g & \boldsymbol{q}_d & \boldsymbol{q}_f \end{bmatrix} \tag{26}$$
$$\boldsymbol{q}_{gb} = \boldsymbol{A}_g \boldsymbol{q}_g \tag{27}$$

where $\boldsymbol{a}_r$ is the $n \times 1$ vector whose generic element $a_{r,i}$ is equal to one if the *ith* bus is the reactive energy reference bus or is equal to zero otherwise. Assuming that the *ith* bus is the reactive energy reference bus, the $(n-1) \times n$ matrix $\boldsymbol{A}_{\bar{r}}$ results from an $n \times n$ identity matrix $\boldsymbol{I}_n$ whose *ith* row is eliminated. The vector of state variables $\boldsymbol{x}$ contains the voltage angles and magnitudes at all buses except those at the EPS slack bus. Equation (20) is the reactive power balance constraint at the reactive energy reference bus, and (21) represents the reactive power balance constraints at buses that are not the reactive energy reference bus. Inequalities (22) and (23) encompass the upper and lower limits of reactive power generation, respectively. Inequalities (24) and (25) comprise the upper and lower bounds of the state variables, respectively.

The Lagrangian function of the OPF problem is given by:

$$\begin{aligned} \mathrm{L} = {} & \mathrm{F}\left(\boldsymbol{p}_{gb}\right) + p_{ds}\lambda_{p_{ds}} + \left[\boldsymbol{s}_{fl} - \boldsymbol{s}_{fl}^{max}\right]^T \boldsymbol{\mu} \\ & + \left[-\boldsymbol{p}_g - \boldsymbol{\alpha} p_{ds} + \boldsymbol{p}_d + \boldsymbol{p}_f\right]^T \boldsymbol{\lambda}_p \\ & + \left[-q_{g,r} + q_{d,r} + q_{f,r}\right] \lambda_{q,r} \\ & + \left[-\boldsymbol{q}_{g,\bar{r}} + \boldsymbol{q}_{d,\bar{r}} + \boldsymbol{q}_{f,\bar{r}}\right]^T \boldsymbol{\lambda}_{q,\bar{r}} \\ & + \left[\boldsymbol{p}_{gb} - \boldsymbol{p}_{gb}^{max}\right]^T \overline{\boldsymbol{\eta}}_p + \left[-\boldsymbol{p}_{gb} + \boldsymbol{p}_{gb}^{min}\right]^T \underline{\boldsymbol{\eta}}_p \\ & + \left[\boldsymbol{q}_{gb} - \boldsymbol{q}_{gb}^{max}\right]^T \overline{\boldsymbol{\eta}}_q + \left[-\boldsymbol{q}_{gb} + \boldsymbol{q}_{gb}^{min}\right]^T \underline{\boldsymbol{\eta}}_q \\ & + \left[\boldsymbol{x} - \boldsymbol{x}^{max}\right]^T \overline{\boldsymbol{\varphi}} + \left[-\boldsymbol{x} + \boldsymbol{x}^{min}\right]^T \underline{\boldsymbol{\varphi}} \end{aligned} \tag{28}$$

where the scalar $\lambda_{q,r}$ corresponds to the element associated with the reactive energy reference bus in vector $\boldsymbol{\lambda}_q$. The vector $\boldsymbol{\lambda}_{q,\bar{r}}$ contains only the elements related to the buses that are not the reactive energy reference bus in vector $\boldsymbol{\lambda}_q$. These relationships can be written as follows:

$$\begin{bmatrix} \lambda_{q,r} \\ \boldsymbol{\lambda}_{q,\bar{r}} \end{bmatrix} = \begin{bmatrix} \boldsymbol{a}_r^T \\ \boldsymbol{A}_{\bar{r}} \end{bmatrix} \boldsymbol{\lambda}_q. \tag{29}$$

The KKT necessary conditions for optimality of the OPF solution are composed of (9) and (11), and the following relations:

$$\frac{\partial \mathrm{L}}{\partial \boldsymbol{q}_{gb}} = -\boldsymbol{\lambda}_{q_{gb}} + \overline{\boldsymbol{\eta}}_q - \underline{\boldsymbol{\eta}}_q = \mathbf{0}_{n_g} \tag{30}$$

$$\begin{aligned} \frac{\partial \mathrm{L}}{\partial \boldsymbol{x}} = {} & \left(\frac{\partial \boldsymbol{p}_f}{\partial \boldsymbol{x}}\right)^T \boldsymbol{\lambda}_p + \left(\frac{\partial \boldsymbol{q}_{f,\bar{r}}}{\partial \boldsymbol{x}}\right)^T \boldsymbol{\lambda}_{q,\bar{r}} + \frac{\partial q_{f,r}}{\partial \boldsymbol{x}} \lambda_{q,r} \\ & + \left(\frac{\partial \boldsymbol{s}_{fl}}{\partial \boldsymbol{x}}\right)^T \boldsymbol{\mu} + \overline{\boldsymbol{\varphi}} - \underline{\boldsymbol{\varphi}} = \mathbf{0}_{2n-2} \end{aligned} \tag{31}$$

where $\boldsymbol{\lambda}_{q_{gb}}$ is the vector containing the reactive power LMPs at the generation buses, and is obtained as follows:

$$\boldsymbol{\lambda}_{q_{gb}} = \boldsymbol{A}_g \boldsymbol{\lambda}_q. \tag{32}$$

By rearranging (11) and (31), it is possible to formulate the matrix relation defined in (33), as shown at the bottom of the page.

Let $\boldsymbol{q}_{\bar{r}} = \boldsymbol{q}_{g,\bar{r}} - \boldsymbol{q}_{d,\bar{r}}$ be the vector containing the net reactive power injections at buses that are not the reactive energy reference bus. To obtain the Jacobian matrix of the power flow equations (3) and (21), relations (3) and (21) are differentiated with respect to $\boldsymbol{p}$ and $\boldsymbol{q}_{\bar{r}}$ as follows:

$$-\frac{\partial \left(\boldsymbol{p}_g - \boldsymbol{p}_d\right)}{\partial \boldsymbol{p}} - \boldsymbol{\alpha}\left(\frac{\partial p_{ds}}{\partial \boldsymbol{p}}\right)^T + \frac{\partial \boldsymbol{p}_f}{\partial \boldsymbol{p}} = \mathbf{0}_{n \times n}$$

$$\begin{aligned} & \begin{bmatrix} \left(\frac{\partial \boldsymbol{p}_f}{\partial \boldsymbol{x}}\right)^T \boldsymbol{\lambda}_p + \left(\frac{\partial \boldsymbol{q}_{f,\bar{r}}}{\partial \boldsymbol{x}}\right)^T \boldsymbol{\lambda}_{q,\bar{r}} \\ -\boldsymbol{\alpha}^T \boldsymbol{\lambda}_p \end{bmatrix} = \begin{bmatrix} -\frac{\partial q_{f,r}}{\partial \boldsymbol{x}} \lambda_{q,r} - \left(\frac{\partial \boldsymbol{s}_{fl}}{\partial \boldsymbol{x}}\right)^T \boldsymbol{\mu} - \overline{\boldsymbol{\varphi}} + \underline{\boldsymbol{\varphi}} \\ -\lambda_{p_{ds}} \end{bmatrix} \\ & \Longrightarrow \begin{bmatrix} \left(\frac{\partial \boldsymbol{p}_f}{\partial \boldsymbol{x}}\right)^T & \left(\frac{\partial \boldsymbol{q}_{f,\bar{r}}}{\partial \boldsymbol{x}}\right)^T \\ -\boldsymbol{\alpha}^T & \mathbf{0}_{n-1}^T \end{bmatrix} \begin{bmatrix} \boldsymbol{\lambda}_p \\ \boldsymbol{\lambda}_{q,\bar{r}} \end{bmatrix} = \begin{bmatrix} -\frac{\partial q_{f,r}}{\partial \boldsymbol{x}} \lambda_{q,r} - \left(\frac{\partial \boldsymbol{s}_{fl}}{\partial \boldsymbol{x}}\right)^T \boldsymbol{\mu} - \overline{\boldsymbol{\varphi}} + \underline{\boldsymbol{\varphi}} \\ -\lambda_{p_{ds}} \end{bmatrix} \\ & \Longrightarrow \begin{bmatrix} \boldsymbol{\lambda}_p \\ \boldsymbol{\lambda}_{q,\bar{r}} \end{bmatrix} = \begin{bmatrix} \begin{bmatrix} \frac{\partial \boldsymbol{p}_f}{\partial \boldsymbol{x}} & -\boldsymbol{\alpha} \\ \frac{\partial \boldsymbol{q}_{f,\bar{r}}}{\partial \boldsymbol{x}} & \mathbf{0}_{n-1} \end{bmatrix}^{-1} \end{bmatrix}^T \begin{bmatrix} -\frac{\partial q_{f,r}}{\partial \boldsymbol{x}} \lambda_{q,r} - \left(\frac{\partial \boldsymbol{s}_{fl}}{\partial \boldsymbol{x}}\right)^T \boldsymbol{\mu} - \overline{\boldsymbol{\varphi}} + \underline{\boldsymbol{\varphi}} \\ -\lambda_{p_{ds}} \end{bmatrix}. \end{aligned} \tag{33}$$

$$\implies -\frac{\partial \boldsymbol{p}}{\partial \boldsymbol{p}} - \boldsymbol{\alpha}\left(\frac{\partial p_{ds}}{\partial \boldsymbol{p}}\right)^T + \frac{\partial \boldsymbol{p}_f}{\partial \boldsymbol{x}}\frac{\partial \boldsymbol{x}}{\partial \boldsymbol{p}} = \mathbf{0}_{n\times n}$$

$$\implies \begin{bmatrix} \frac{\partial \boldsymbol{p}_f}{\partial \boldsymbol{x}} & -\boldsymbol{\alpha} \end{bmatrix} \begin{bmatrix} \frac{\partial \boldsymbol{x}}{\partial \boldsymbol{p}} \\ \left(\frac{\partial p_{ds}}{\partial \boldsymbol{p}}\right)^T \end{bmatrix} = \boldsymbol{I}_n \tag{34}$$

$$-\boldsymbol{\alpha}\left(\frac{\partial p_{ds}}{\partial \boldsymbol{q}_{\bar{r}}}\right)^T + \frac{\partial \boldsymbol{p}_f}{\partial \boldsymbol{q}_{\bar{r}}} = \mathbf{0}_{n\times(n-1)}$$

$$\implies -\boldsymbol{\alpha}\left(\frac{\partial p_{ds}}{\partial \boldsymbol{q}_{\bar{r}}}\right)^T + \frac{\partial \boldsymbol{p}_f}{\partial \boldsymbol{x}}\frac{\partial \boldsymbol{x}}{\partial \boldsymbol{q}_{\bar{r}}} = \mathbf{0}_{n\times(n-1)}$$

$$\implies \begin{bmatrix} \frac{\partial \boldsymbol{p}_f}{\partial \boldsymbol{x}} & -\boldsymbol{\alpha} \end{bmatrix} \begin{bmatrix} \frac{\partial \boldsymbol{x}}{\partial \boldsymbol{q}_{\bar{r}}} \\ \left(\frac{\partial p_{ds}}{\partial \boldsymbol{q}_{\bar{r}}}\right)^T \end{bmatrix} = \mathbf{0}_{n\times(n-1)} \tag{35}$$

$$\frac{\partial \boldsymbol{q}_{f,\bar{r}}}{\partial \boldsymbol{p}} = \mathbf{0}_{(n-1)\times n} \implies \frac{\partial \boldsymbol{q}_{f,\bar{r}}}{\partial \boldsymbol{x}}\frac{\partial \boldsymbol{x}}{\partial \boldsymbol{p}} = \mathbf{0}_{(n-1)\times n} \tag{36}$$

$$-\frac{\partial\left(\boldsymbol{q}_{g,\bar{r}} - \boldsymbol{q}_{d,\bar{r}}\right)}{\partial \boldsymbol{q}_{\bar{r}}} + \frac{\partial \boldsymbol{q}_{f,\bar{r}}}{\partial \boldsymbol{q}_{\bar{r}}} = \mathbf{0}_{(n-1)\times(n-1)}$$

$$\implies -\frac{\partial \boldsymbol{q}_{\bar{r}}}{\partial \boldsymbol{q}_{\bar{r}}} + \frac{\partial \boldsymbol{q}_{f,\bar{r}}}{\partial \boldsymbol{x}}\frac{\partial \boldsymbol{x}}{\partial \boldsymbol{q}_{\bar{r}}} = \mathbf{0}_{(n-1)\times(n-1)}$$

$$\implies \frac{\partial \boldsymbol{q}_{f,\bar{r}}}{\partial \boldsymbol{x}}\frac{\partial \boldsymbol{x}}{\partial \boldsymbol{q}_{\bar{r}}} = \boldsymbol{I}_{n-1}. \tag{37}$$

Equations (34)–(37) can be combined to form the Jacobian matrix, as follows:

$$\begin{bmatrix} \frac{\partial \boldsymbol{p}_f}{\partial \boldsymbol{x}} & -\boldsymbol{\alpha} \\ \frac{\partial \boldsymbol{q}_{f,\bar{r}}}{\partial \boldsymbol{x}} & \mathbf{0}_{n-1} \end{bmatrix} = \begin{bmatrix} \frac{\partial \boldsymbol{x}}{\partial \boldsymbol{p}} & \frac{\partial \boldsymbol{x}}{\partial \boldsymbol{q}_{\bar{r}}} \\ \left(\frac{\partial p_{ds}}{\partial \boldsymbol{p}}\right)^T & \left(\frac{\partial p_{ds}}{\partial \boldsymbol{q}_{\bar{r}}}\right)^T \end{bmatrix}^{-1}. \tag{38}$$

Substituting (38) into (33) gives (39), as shown at the bottom of the page.

The active power transmission losses can be computed using (16), and the reactive power transmission losses are calculated as follows:

$$q_l = \mathbf{1}_{n-1}^T \boldsymbol{q}_{\bar{r}} + q_{g,r} - q_{d,r}. \tag{40}$$

Differentiating (16) with respect to $\boldsymbol{q}_{\bar{r}}$ and differentiating (40) with respect to $\boldsymbol{p}$ and $\boldsymbol{q}_{\bar{r}}$ yields

$$\frac{\partial p_l}{\partial \boldsymbol{q}_{\bar{r}}} = \frac{\partial p_{ds}}{\partial \boldsymbol{q}_{\bar{r}}} \tag{41}$$

$$\frac{\partial q_l}{\partial \boldsymbol{p}} = \frac{\partial q_{g,r}}{\partial \boldsymbol{p}} = \frac{\partial\left(q_{d,r} + q_{f,r}\right)}{\partial \boldsymbol{p}} = \frac{\partial q_{f,r}}{\partial \boldsymbol{p}} \tag{42}$$

$$\frac{\partial q_l}{\partial \boldsymbol{q}_{\bar{r}}} = \mathbf{1}_{n-1} + \frac{\partial q_{g,r}}{\partial \boldsymbol{q}_{\bar{r}}} = \mathbf{1}_{n-1} + \frac{\partial\left(q_{d,r} + q_{f,r}\right)}{\partial \boldsymbol{q}_{\bar{r}}} = \mathbf{1}_{n-1} + \frac{\partial q_{f,r}}{\partial \boldsymbol{q}_{\bar{r}}}. \tag{43}$$

By grouping (17) and (41)–(43), the matrix containing the active and reactive power loss sensitivity factors is obtained as:

$$\begin{bmatrix} \frac{\partial p_{ds}}{\partial \boldsymbol{p}} & \frac{\partial q_{f,r}}{\partial \boldsymbol{p}} \\ \frac{\partial p_{ds}}{\partial \boldsymbol{q}_{\bar{r}}} & \frac{\partial q_{f,r}}{\partial \boldsymbol{q}_{\bar{r}}} \end{bmatrix} = \begin{bmatrix} -\mathbf{1}_n + \frac{\partial p_l}{\partial \boldsymbol{p}} & \frac{\partial q_l}{\partial \boldsymbol{p}} \\ \frac{\partial p_l}{\partial \boldsymbol{q}_{\bar{r}}} & -\mathbf{1}_{n-1} + \frac{\partial q_l}{\partial \boldsymbol{q}_{\bar{r}}} \end{bmatrix}. \tag{44}$$

Substituting (44) into (39) gives

$$\begin{bmatrix} \boldsymbol{\lambda}_p \\ \boldsymbol{\lambda}_{q,\bar{r}} \end{bmatrix} = \begin{bmatrix} \mathbf{1}_n - \frac{\partial p_l}{\partial \boldsymbol{p}} & -\frac{\partial q_l}{\partial \boldsymbol{p}} \\ -\frac{\partial p_l}{\partial \boldsymbol{q}_{\bar{r}}} & \mathbf{1}_{n-1} - \frac{\partial q_l}{\partial \boldsymbol{q}_{\bar{r}}} \end{bmatrix} \begin{bmatrix} \lambda_{p_{ds}} \\ \lambda_{q,r} \end{bmatrix} - \begin{bmatrix} \left(\frac{\partial \boldsymbol{s}_{fl}}{\partial \boldsymbol{p}}\right)^T \\ \left(\frac{\partial \boldsymbol{s}_{fl}}{\partial \boldsymbol{q}_{\bar{r}}}\right)^T \end{bmatrix} \boldsymbol{\mu} - \begin{bmatrix} \left(\frac{\partial \boldsymbol{x}}{\partial \boldsymbol{p}}\right)^T \\ \left(\frac{\partial \boldsymbol{x}}{\partial \boldsymbol{q}_{\bar{r}}}\right)^T \end{bmatrix} \left[\overline{\boldsymbol{\varphi}} - \underline{\boldsymbol{\varphi}}\right]. \tag{45}$$

In current LMP-based market practices, financial settlements are mostly carried out through active power LMPs. Thus, based on (45), the active power LMPs can

$$\begin{aligned} \begin{bmatrix} \boldsymbol{\lambda}_p \\ \boldsymbol{\lambda}_{q,\bar{r}} \end{bmatrix} &= \begin{bmatrix} \left(\frac{\partial \boldsymbol{x}}{\partial \boldsymbol{p}}\right)^T & \frac{\partial p_{ds}}{\partial \boldsymbol{p}} \\ \left(\frac{\partial \boldsymbol{x}}{\partial \boldsymbol{q}_{\bar{r}}}\right)^T & \frac{\partial p_{ds}}{\partial \boldsymbol{q}_{\bar{r}}} \end{bmatrix} \begin{bmatrix} -\frac{\partial q_{f,r}}{\partial \boldsymbol{x}}\lambda_{q,r} - \left(\frac{\partial \boldsymbol{s}_{fl}}{\partial \boldsymbol{x}}\right)^T \boldsymbol{\mu} - \overline{\boldsymbol{\varphi}} + \underline{\boldsymbol{\varphi}} \\ -\lambda_{p_{ds}} \end{bmatrix} \\ &= -\begin{bmatrix} \frac{\partial p_{ds}}{\partial \boldsymbol{p}} & \left(\frac{\partial \boldsymbol{x}}{\partial \boldsymbol{p}}\right)^T \frac{\partial q_{f,r}}{\partial \boldsymbol{x}} \\ \frac{\partial p_{ds}}{\partial \boldsymbol{q}_{\bar{r}}} & \left(\frac{\partial \boldsymbol{x}}{\partial \boldsymbol{q}_{\bar{r}}}\right)^T \frac{\partial q_{f,r}}{\partial \boldsymbol{x}} \end{bmatrix} \begin{bmatrix} \lambda_{p_{ds}} \\ \lambda_{q,r} \end{bmatrix} + \begin{bmatrix} \left(\frac{\partial \boldsymbol{x}}{\partial \boldsymbol{p}}\right)^T \\ \left(\frac{\partial \boldsymbol{x}}{\partial \boldsymbol{q}_{\bar{r}}}\right)^T \end{bmatrix} \left[-\left(\frac{\partial \boldsymbol{s}_{fl}}{\partial \boldsymbol{x}}\right)^T \boldsymbol{\mu} - \overline{\boldsymbol{\varphi}} + \underline{\boldsymbol{\varphi}}\right] \\ &= -\begin{bmatrix} \frac{\partial p_{ds}}{\partial \boldsymbol{p}} & \frac{\partial q_{f,r}}{\partial \boldsymbol{p}} \\ \frac{\partial p_{ds}}{\partial \boldsymbol{q}_{\bar{r}}} & \frac{\partial q_{f,r}}{\partial \boldsymbol{q}_{\bar{r}}} \end{bmatrix} \begin{bmatrix} \lambda_{p_{ds}} \\ \lambda_{q,r} \end{bmatrix} + \begin{bmatrix} -\left(\frac{\partial \boldsymbol{s}_{fl}}{\partial \boldsymbol{p}}\right)^T \\ -\left(\frac{\partial \boldsymbol{s}_{fl}}{\partial \boldsymbol{q}_{\bar{r}}}\right)^T \end{bmatrix} \boldsymbol{\mu} + \begin{bmatrix} \left(\frac{\partial \boldsymbol{x}}{\partial \boldsymbol{p}}\right)^T \\ \left(\frac{\partial \boldsymbol{x}}{\partial \boldsymbol{q}_{\bar{r}}}\right)^T \end{bmatrix} \left[-\overline{\boldsymbol{\varphi}} + \underline{\boldsymbol{\varphi}}\right]. \end{aligned} \tag{39}$$

be written as:

$$\boldsymbol{\lambda}_p = \underbrace{\mathbf{1}_n \lambda_{p_{ds}}}_{\boldsymbol{\lambda}_p^e} \underbrace{- \frac{\partial p_l}{\partial \boldsymbol{p}} \lambda_{p_{ds}}}_{\boldsymbol{\lambda}_p^{pl}} \underbrace{- \frac{\partial q_l}{\partial \boldsymbol{p}} \lambda_{q,r}}_{\boldsymbol{\lambda}_p^{ql}} \underbrace{- \left(\frac{\partial s_{fl}}{\partial \boldsymbol{p}}\right)^T \boldsymbol{\mu}}_{\boldsymbol{\lambda}_p^c} \underbrace{- \left(\frac{\partial x}{\partial \boldsymbol{p}}\right)^T \left[\overline{\boldsymbol{\phi}} - \underline{\boldsymbol{\phi}}\right]}_{\boldsymbol{\lambda}_p^x}. \tag{46}$$

In this way, (46) gives the five LMP components from the decomposition approach based on the conventional active power distributed slack scheme and the traditional single bus reactive power slack model.

C. CAVEATS

There is a lack of homogeneity in the literature regarding the definition of the power class (injection or demand) used in the differentiation of the power flow equations that govern the computation of the LMP components. For example, the decomposition model described in [23] is based on sensitivities with respect to the power demand, whereas the approach proposed in [6] is governed by sensitivities with respect to the power injection. In the current paper, all decomposition models are based on a broader sensitivity approach, which considers the differentiation of power flow equations with respect to net power injections.

Throughout the mathematical derivation of the decomposition approach in Section II-B, the equalities (3), (16), (21), and (40) were differentiated with respect to $\boldsymbol{p}$ and $\boldsymbol{q}_{\overline{r}}$. However, if (3), (16), (21), and (40) are differentiated with respect to $\boldsymbol{p}_d$ and $\boldsymbol{q}_{d,\overline{r}}$, it is possible to obtain the following LMP decomposition:

$$\boldsymbol{\lambda}_p = \mathbf{1}_n \lambda_{p_{ds}} + \frac{\partial p_l}{\partial \boldsymbol{p}_d} \lambda_{p_{ds}} + \frac{\partial q_l}{\partial \boldsymbol{p}_d} \lambda_{q,r} + \left(\frac{\partial \boldsymbol{s}_{fl}}{\partial \boldsymbol{p}_d}\right)^T \boldsymbol{\mu} + \left(\frac{\partial \boldsymbol{x}}{\partial \boldsymbol{p}_d}\right)^T \left[\overline{\boldsymbol{\varphi}} - \underline{\boldsymbol{\varphi}}\right]. \tag{47}$$

However, observing that

$$\begin{bmatrix} \dfrac{\partial \boldsymbol{x}}{\partial \boldsymbol{p}} & \dfrac{\partial \boldsymbol{x}}{\partial \boldsymbol{q}_{\overline{r}}} \\ \left(\dfrac{\partial p_{ds}}{\partial \boldsymbol{p}}\right)^T & \left(\dfrac{\partial p_{ds}}{\partial \boldsymbol{q}_{\overline{r}}}\right)^T \end{bmatrix} = - \begin{bmatrix} \dfrac{\partial \boldsymbol{x}}{\partial \boldsymbol{p}_d} & \dfrac{\partial \boldsymbol{x}}{\partial \boldsymbol{q}_{d,\overline{r}}} \\ \left(\dfrac{\partial p_{ds}}{\partial \boldsymbol{p}_d}\right)^T & \left(\dfrac{\partial p_{ds}}{\partial \boldsymbol{q}_{d,\overline{r}}}\right)^T \end{bmatrix} \tag{48}$$

it can be concluded that the LMP components of the decomposition models in (46) and (47) are identical. If the same procedures used to derive (47) and (48) are adopted in the scope of the sensitivities with respect to $\boldsymbol{p}_g$ and $\boldsymbol{q}_{g,\overline{r}}$, the same equivalence will be identified. Thus, decomposition models based on the proposed sensitivities with respect to net power injection, and on the conventional sensitivities with respect to power injection or demand, provide the same LMP components.

This paper proposes a decomposition scheme based on the incorporation of a new reactive power distributed slack model. However, traditional power flow formulations are already based on a distributed reactive power slack scheme in which mismatches between reactive power generation, load, and losses are counterbalanced in conventional slack and PV buses. In OPF frameworks, bus categorization represents an excessive modelling practice that limits the feasible possibilities for OPF problem formulation and solutions [36]. Despite the possibility of incorporating the reactive power distributed compensation scheme based on slack and PV buses in the OPF formulations, it is impossible to design LMP decomposition models corresponding to such formulations considering current market practices. To demonstrate this impossibility, it is now considered that the compensation of reactive power mismatches is no longer performed solely on a reactive energy reference bus (the approach used in Section II-B), but on slack and PV buses. Thus, the slack and PV buses can be considered as a type of reactive power distributed slack bus and can be assumed to be the reactive energy reference bus. In this context, the OPF model is given by:

$$\min \ \mathrm{F}\left(\boldsymbol{p}_{gb}\right) \tag{49}$$

$$\text{s.t.} \ -q_{g,s} + q_{d,s} + q_{f,s} = 0 \tag{50}$$

$$-\boldsymbol{q}_{g,pv} + \boldsymbol{q}_{d,pv} + \boldsymbol{q}_{f,pv} = \mathbf{0}_{n_{pv}} \tag{51}$$

$$-\boldsymbol{q}_{g,\overline{spv}} + \boldsymbol{q}_{d,\overline{spv}} + \boldsymbol{q}_{f,\overline{spv}} = \mathbf{0}_{n-1-n_{pv}} \tag{52}$$

$$\boldsymbol{x}_{\overline{spv}} - \boldsymbol{x}_{\overline{spv}}^{max} \leq \mathbf{0}_{2n-2-n_{pv}} \tag{53}$$

$$-\boldsymbol{x}_{\overline{spv}} + \boldsymbol{x}_{\overline{spv}}^{min} \leq \mathbf{0}_{2n-2-n_{pv}} \tag{54}$$

$$(2)\text{–}(6) \text{ and } (22)\text{–}(25)$$

where $q_{g,s}$, $q_{d,s}$, and $q_{f,s}$ represent only the elements associated with the slack bus in vectors $\boldsymbol{q}_g$, $\boldsymbol{q}_d$, and $\boldsymbol{q}_f$, respectively. The vectors $\boldsymbol{q}_{g,pv}$, $\boldsymbol{q}_{d,pv}$, and $\boldsymbol{q}_{f,pv}$ contain only the elements associated with the PV buses in vectors $\boldsymbol{q}_g$, $\boldsymbol{q}_d$, and $\boldsymbol{q}_f$, respectively. The vectors $\boldsymbol{q}_{g,\overline{spv}}$, $\boldsymbol{q}_{d,\overline{spv}}$, and $\boldsymbol{q}_{f,\overline{spv}}$ contain only the elements associated with buses that are not slack or PV buses in vectors $\boldsymbol{q}_g$, $\boldsymbol{q}_d$, and $\boldsymbol{q}_f$, respectively. Therefore, these relations can be written as:

$$\begin{bmatrix} q_{g,s} & q_{d,s} & q_{f,s} \\ \boldsymbol{q}_{g,pv} & \boldsymbol{q}_{d,pv} & \boldsymbol{q}_{f,pv} \\ \boldsymbol{q}_{g,\overline{spv}} & \boldsymbol{q}_{d,\overline{spv}} & \boldsymbol{q}_{f,\overline{spv}} \end{bmatrix} = \begin{bmatrix} \boldsymbol{a}_s^T \\ \boldsymbol{A}_{pv} \\ \boldsymbol{A}_{\overline{spv}} \end{bmatrix} \begin{bmatrix} \boldsymbol{q}_g & \boldsymbol{q}_d & \boldsymbol{q}_f \end{bmatrix} \tag{55}$$

where $\boldsymbol{a}_s$ is the $n \times 1$ vector whose generic element $a_{s,i}$ is equal to one if the *ith* bus is the slack bus, and is equal to zero otherwise. Assuming that Ω is the set containing the indices of those buses that are not PV buses, the $n_{pv} \times n$ matrix $\boldsymbol{A}_{pv}$ is the one resulting from an $n \times n$ identity matrix $\boldsymbol{I}_n$ whose *ith* rows are eliminated $\forall i \in \Omega$. Similarly, assuming that Υ is the set of slack and PV bus indices, the $\left(n - n_{pv} - 1\right) \times n$ matrix $\boldsymbol{A}_{\overline{spv}}$ is the one resulting from a $n \times n$ identity matrix $\boldsymbol{I}_n$ whose *ith* rows are eliminated $\forall i \in \Upsilon$. The vector of state

variables $\boldsymbol{x}_{\overline{spv}}$ contains the voltage angles at all buses, except the slack bus, and the voltage magnitudes at all buses, except the slack and PV buses. Equations (50) and (51) represent the reactive power balance constraints at the slack and PV buses, respectively. Equation (52) encompasses the reactive power balance constraints at buses that are not slack or PV buses.

Let $\boldsymbol{q}_{\overline{spv}} = \boldsymbol{q}_{g,\overline{spv}} - \boldsymbol{q}_{d,\overline{spv}}$ be the vector containing the net reactive power injections at buses that are not slack or PV buses. Following procedures analogous to those used in the formulation of (38), by differentiating (3) and (52) with respect to $\boldsymbol{p}$ and $\boldsymbol{q}_{\overline{spv}}$, the Jacobian matrix of the power flow equations (3) and (52) can be derived as:

$$\begin{bmatrix} \dfrac{\partial \boldsymbol{p}_f}{\partial \boldsymbol{x}_{\overline{spv}}} & -\boldsymbol{\alpha} \\ \dfrac{\partial \boldsymbol{q}_{f,\overline{spv}}}{\partial \boldsymbol{x}_{\overline{spv}}} & \boldsymbol{0}_{n-1-n_{pv}} \end{bmatrix} = \begin{bmatrix} \dfrac{\partial \boldsymbol{x}_{\overline{spv}}}{\partial \boldsymbol{p}} & \dfrac{\partial \boldsymbol{x}_{\overline{spv}}}{\partial \boldsymbol{q}_{\overline{spv}}} \\ \left(\dfrac{\partial p_{ds}}{\partial \boldsymbol{p}}\right)^T & \left(\dfrac{\partial p_{ds}}{\partial \boldsymbol{q}_{\overline{spv}}}\right)^T \end{bmatrix}^{-1}. \tag{56}$$

The active power transmission losses are calculated using (16), and the reactive power transmission losses are computed as:

$$\begin{aligned} q_l = {} & \boldsymbol{1}_{n-1-n_{pv}}^T \boldsymbol{q}_{\overline{spv}} + q_{g,s} - q_{d,s} + \boldsymbol{1}_{n_{pv}}^T \boldsymbol{q}_{g,pv} \\ & - \boldsymbol{1}_{n_{pv}}^T \boldsymbol{q}_{d,pv}. \end{aligned} \tag{57}$$

Following steps similar to those employed in the derivation of (44), by differentiating (16) and (57) with respect to $\boldsymbol{p}$ and $\boldsymbol{q}_{\overline{spv}}$, the matrix containing the active and reactive power loss sensitivity factors is formulated in (58), as shown at the bottom of the page.

Taking steps analogous to those used in LMP decomposition (39), the following relationship can be obtained:

$$\begin{aligned} \begin{bmatrix} \boldsymbol{\lambda}_p \\ \boldsymbol{\lambda}_{q,\overline{spv}} \end{bmatrix} = {} & - \begin{bmatrix} \dfrac{\partial p_{ds}}{\partial \boldsymbol{p}} & \dfrac{\partial q_{f,s}}{\partial \boldsymbol{p}} & \left(\dfrac{\partial \boldsymbol{q}_{f,pv}}{\partial \boldsymbol{p}}\right)^T \\ \dfrac{\partial p_{ds}}{\partial \boldsymbol{q}_{\overline{spv}}} & \dfrac{\partial q_{f,s}}{\partial \boldsymbol{q}_{\overline{spv}}} & \left(\dfrac{\partial \boldsymbol{q}_{f,pv}}{\partial \boldsymbol{q}_{\overline{spv}}}\right)^T \end{bmatrix} \begin{bmatrix} \lambda_{p_{ds}} \\ \lambda_{q,s} \\ \boldsymbol{\lambda}_{q,pv} \end{bmatrix} \\ & - \begin{bmatrix} \left(\dfrac{\partial \boldsymbol{s}_{fl}}{\partial \boldsymbol{p}}\right)^T \\ \left(\dfrac{\partial \boldsymbol{s}_{fl}}{\partial \boldsymbol{q}_{\overline{spv}}}\right)^T \end{bmatrix} \boldsymbol{\mu} + \begin{bmatrix} \left(\dfrac{\partial \boldsymbol{x}}{\partial \boldsymbol{p}}\right)^T \\ \left(\dfrac{\partial \boldsymbol{x}}{\partial \boldsymbol{q}_{\overline{spv}}}\right)^T \end{bmatrix} \\ & \times \left[-\overline{\boldsymbol{\varphi}} + \underline{\boldsymbol{\varphi}}\right] \end{aligned} \tag{59}$$

where the scalar $\lambda_{q,s}$ is the element associated with the slack bus in vector $\boldsymbol{\lambda}_q$. The vector $\boldsymbol{\lambda}_{q,pv}$ is formed by the elements associated with the PV buses in vector $\boldsymbol{\lambda}_q$. The vector $\boldsymbol{\lambda}_{q,\overline{spv}}$ contains only the elements associated with the buses that are not slack or PV buses in vector $\boldsymbol{\lambda}_q$. These relationships are given by:

$$\begin{bmatrix} \lambda_{q,s} \\ \boldsymbol{\lambda}_{q,pv} \\ \boldsymbol{\lambda}_{q,\overline{spv}} \end{bmatrix} = \begin{bmatrix} \boldsymbol{a}_s^T \\ \boldsymbol{A}_{pv} \\ \boldsymbol{A}_{\overline{spv}} \end{bmatrix} \boldsymbol{\lambda}_q. \tag{60}$$

It is possible to substitute (58) into (59) only if $\boldsymbol{1}_{n_{pv}} \lambda_{q,s} = \boldsymbol{\lambda}_{q,pv}$, which makes such a decomposition unfeasible for market practices, as it requires that the reactive power LMPs of all slack and PV buses are always identical.

III. PROPOSED LMP DECOMPOSITION MODEL

The proposed LMP decomposition approach is based on an OPF formulation integrated with a fully distributed slack bus model. In this approach, the active power mismatch compensation scheme follows the formulation presented in Section II-A, and the reactive power mismatch compensation is performed using a proposed reactive power distributed slack bus model. Despite modelling challenges similar to those in the decomposition approach of Section II-B concerning the implementation of post-optimization sensitivity vectors, the proposed decomposition model offers infinite possibilities for reactive power compensation strategies, including the one in Section II-B. An overview of the compensation frameworks to offset mismatches between generation, load, and losses used in LMP decomposition models in the literature is illustrated in Fig. 1. The OPF framework that governs the proposed LMP decomposition model is defined as:

$$\min \ \mathrm{F}\left(\boldsymbol{p}_{gb}\right) \tag{61}$$

$$\text{s.t. } q_{ds} = 0 \tag{62}$$

$$-\boldsymbol{q}_g - \boldsymbol{\beta} q_{ds} + \boldsymbol{q}_d + \boldsymbol{q}_f = \boldsymbol{0}_n \tag{63}$$

$$(2)\text{–}(6) \text{ and } (22)\text{–}(25).$$

A reactive power distributed slack bus integrated into a power flow model is a fictitious node that exists only in the scope of mathematical formulation. For optimization purposes, the reactive power injection into the reactive power distributed slack bus must be zero, as indicated by constraint (62). However, in power flow applications or *ex post* sensitivity analysis used in deriving LMP components, mismatches compensated through injections in the reactive power distributed slack bus are considered. The amount of reactive power injected into the reactive power distributed slack bus is distributed among all the EPS buses based on the proportion defined by the participation factors of

$$\begin{bmatrix} \dfrac{\partial p_{ds}}{\partial \boldsymbol{p}} & \dfrac{\partial q_{f,s}}{\partial \boldsymbol{p}} + \left(\dfrac{\partial \boldsymbol{q}_{f,pv}}{\partial \boldsymbol{p}}\right)^T \boldsymbol{1}_{n_{pv}} \\ \dfrac{\partial p_{ds}}{\partial \boldsymbol{q}_{\overline{spv}}} & \dfrac{\partial q_{f,s}}{\partial \boldsymbol{q}_{\overline{spv}}} + \left(\dfrac{\partial \boldsymbol{q}_{f,pv}}{\partial \boldsymbol{q}_{\overline{spv}}}\right)^T \boldsymbol{1}_{n_{pv}} \end{bmatrix} = \begin{bmatrix} -\boldsymbol{1}_n + \dfrac{\partial p_l}{\partial \boldsymbol{p}} & \dfrac{\partial q_l}{\partial \boldsymbol{p}} \\ \dfrac{\partial p_l}{\partial \boldsymbol{q}_{\overline{spv}}} & -\boldsymbol{1}_{n-1-n_{pv}} + \dfrac{\partial q_l}{\partial \boldsymbol{q}_{\overline{spv}}} \end{bmatrix} \tag{58}$$

vector $\boldsymbol{\beta}$. Equation (63) represents the reactive power balance constraints for all buses.

The Lagrange function of the proposed OPF problem can be formulated as:

$$\begin{aligned}\mathrm{L} = {} & \mathrm{F}\left(\boldsymbol{p}_{gb}\right) + p_{ds}\lambda_{p_{ds}} + q_{ds}\lambda_{q_{ds}} \\ & + \left[\boldsymbol{s}_{fl} - \boldsymbol{s}_{fl}^{max}\right]^T \boldsymbol{\mu} \\ & + \left[-\boldsymbol{p}_g - \boldsymbol{\alpha} p_{ds} + \boldsymbol{p}_d + \boldsymbol{p}_f\right]^T \boldsymbol{\lambda}_p \\ & + \left[-\boldsymbol{q}_g - \boldsymbol{\beta} q_{ds} + \boldsymbol{q}_d + \boldsymbol{q}_f\right]^T \boldsymbol{\lambda}_q \\ & + \left[\boldsymbol{p}_{gb} - \boldsymbol{p}_{gb}^{max}\right]^T \overline{\boldsymbol{\eta}}_p + \left[-\boldsymbol{p}_{gb} + \boldsymbol{p}_{gb}^{min}\right]^T \underline{\boldsymbol{\eta}}_p \\ & + \left[\boldsymbol{q}_{gb} - \boldsymbol{q}_{gb}^{max}\right]^T \overline{\boldsymbol{\eta}}_q + \left[-\boldsymbol{q}_{gb} + \boldsymbol{q}_{gb}^{min}\right]^T \underline{\boldsymbol{\eta}}_q \\ & + \left[\boldsymbol{x} - \boldsymbol{x}^{max}\right]^T \overline{\boldsymbol{\varphi}} + \left[-\boldsymbol{x} + \boldsymbol{x}^{min}\right]^T \underline{\boldsymbol{\varphi}}. \end{aligned} \tag{64}$$

The KKT necessary conditions for optimality of the OPF solution are composed of (9), (11), and (30), and the following equalities:

$$\begin{aligned}\frac{\partial \mathrm{L}}{\partial \boldsymbol{x}} = {} & \left(\frac{\partial \boldsymbol{p}_f}{\partial \boldsymbol{x}}\right)^T \boldsymbol{\lambda}_p + \left(\frac{\partial \boldsymbol{q}_f}{\partial \boldsymbol{x}}\right)^T \boldsymbol{\lambda}_q + \left(\frac{\partial \boldsymbol{s}_{fl}}{\partial \boldsymbol{x}}\right)^T \boldsymbol{\mu} + \overline{\boldsymbol{\varphi}} \\ & - \underline{\boldsymbol{\varphi}} = \mathbf{0}_{2n-2} \end{aligned} \tag{65}$$

$$\frac{\partial \mathrm{L}}{\partial q_{ds}} = \lambda_{q_{ds}} - \boldsymbol{\beta}^T \boldsymbol{\lambda}_q = 0. \tag{66}$$

Combining (11), (65), and (66) in matrix form, it is possible to obtain the relation defined in (67), as shown at the bottom of the page.

To calculate the Jacobian matrix of the power flow equations (3) and (63), the relation (3) is differentiated with respect to $\boldsymbol{q}$, while (63) is differentiated with respect to $\boldsymbol{p}$ and $\boldsymbol{q}$ as follows:

$$-\boldsymbol{\alpha}\left(\frac{\partial p_{ds}}{\partial \boldsymbol{q}}\right)^T + \frac{\partial \boldsymbol{p}_f}{\partial \boldsymbol{q}} = \mathbf{0}_{n\times n}$$

$$\implies -\boldsymbol{\alpha}\left(\frac{\partial p_{ds}}{\partial \boldsymbol{q}}\right)^T + \frac{\partial \boldsymbol{p}_f}{\partial \boldsymbol{x}}\frac{\partial \boldsymbol{x}}{\partial \boldsymbol{q}} = \mathbf{0}_{n\times n}$$

$$\implies \begin{bmatrix} \dfrac{\partial \boldsymbol{p}_f}{\partial \boldsymbol{x}} & -\boldsymbol{\alpha} \end{bmatrix} \begin{bmatrix} \dfrac{\partial \boldsymbol{x}}{\partial \boldsymbol{q}} \\ \left(\dfrac{\partial p_{ds}}{\partial \boldsymbol{q}}\right)^T \end{bmatrix} = \mathbf{0}_{n\times n} \tag{68}$$

$$-\boldsymbol{\beta}\left(\frac{\partial q_{ds}}{\partial \boldsymbol{p}}\right)^T + \frac{\partial \boldsymbol{q}_f}{\partial \boldsymbol{p}} = \mathbf{0}_{n\times n}$$

$$\implies -\boldsymbol{\beta}\left(\frac{\partial q_{ds}}{\partial \boldsymbol{p}}\right)^T + \frac{\partial \boldsymbol{q}_f}{\partial \boldsymbol{x}}\frac{\partial \boldsymbol{x}}{\partial \boldsymbol{p}} = \mathbf{0}_{n\times n}$$

$$\implies \begin{bmatrix} \dfrac{\partial \boldsymbol{q}_f}{\partial \boldsymbol{x}} & -\boldsymbol{\beta} \end{bmatrix} \begin{bmatrix} \dfrac{\partial \boldsymbol{x}}{\partial \boldsymbol{p}} \\ \left(\dfrac{\partial q_{ds}}{\partial \boldsymbol{p}}\right)^T \end{bmatrix} = \mathbf{0}_{n\times n} \tag{69}$$

$$-\frac{\partial\left(\boldsymbol{q}_g - \boldsymbol{q}_d\right)}{\partial \boldsymbol{q}} - \boldsymbol{\beta}\left(\frac{\partial q_{ds}}{\partial \boldsymbol{q}}\right)^T + \frac{\partial \boldsymbol{q}_f}{\partial \boldsymbol{q}} = \mathbf{0}_{n\times n}$$

$$\implies -\frac{\partial \boldsymbol{q}}{\partial \boldsymbol{q}} - \boldsymbol{\beta}\left(\frac{\partial q_{ds}}{\partial \boldsymbol{q}}\right)^T + \frac{\partial \boldsymbol{q}_f}{\partial \boldsymbol{x}}\frac{\partial \boldsymbol{x}}{\partial \boldsymbol{q}} = \mathbf{0}_{n\times n}$$

$$\implies \begin{bmatrix} \dfrac{\partial \boldsymbol{q}_f}{\partial \boldsymbol{x}} & -\boldsymbol{\beta} \end{bmatrix} \begin{bmatrix} \dfrac{\partial \boldsymbol{x}}{\partial \boldsymbol{q}} \\ \left(\dfrac{\partial q_{ds}}{\partial \boldsymbol{q}}\right)^T \end{bmatrix} = \boldsymbol{I}_n. \tag{70}$$

Combining (34) and (68)–(70) in matrix form, it is possible to obtain the Jacobian matrix as follows:

$$\begin{bmatrix} \dfrac{\partial \boldsymbol{p}_f}{\partial \boldsymbol{x}} & -\boldsymbol{\alpha} & \mathbf{0}_n \\ \dfrac{\partial \boldsymbol{q}_f}{\partial \boldsymbol{x}} & \mathbf{0}_n & -\boldsymbol{\beta} \end{bmatrix} = \begin{bmatrix} \dfrac{\partial \boldsymbol{x}}{\partial \boldsymbol{p}} & \dfrac{\partial \boldsymbol{x}}{\partial \boldsymbol{q}} \\ \left(\dfrac{\partial p_{ds}}{\partial \boldsymbol{p}}\right)^T & \left(\dfrac{\partial p_{ds}}{\partial \boldsymbol{q}}\right)^T \\ \left(\dfrac{\partial q_{ds}}{\partial \boldsymbol{p}}\right)^T & \left(\dfrac{\partial q_{ds}}{\partial \boldsymbol{q}}\right)^T \end{bmatrix}^{-1}. \tag{71}$$

Substituting (71) into (67) gives (72), as shown at the bottom of the next page. The transmission active power losses

$$\begin{bmatrix} \left(\dfrac{\partial \boldsymbol{p}_f}{\partial \boldsymbol{x}}\right)^T \boldsymbol{\lambda}_p + \left(\dfrac{\partial \boldsymbol{q}_f}{\partial \boldsymbol{x}}\right)^T \boldsymbol{\lambda}_q \\ -\boldsymbol{\alpha}^T \boldsymbol{\lambda}_p \\ -\boldsymbol{\beta}^T \boldsymbol{\lambda}_q \end{bmatrix} = \begin{bmatrix} -\left(\dfrac{\partial \boldsymbol{s}_{fl}}{\partial \boldsymbol{x}}\right)^T \boldsymbol{\mu} - \overline{\boldsymbol{\varphi}} + \underline{\boldsymbol{\varphi}} \\ -\lambda_{p_{ds}} \\ -\lambda_{q_{ds}} \end{bmatrix}$$

$$\implies \begin{bmatrix} \left(\dfrac{\partial \boldsymbol{p}_f}{\partial \boldsymbol{x}}\right)^T & \left(\dfrac{\partial \boldsymbol{q}_f}{\partial \boldsymbol{x}}\right)^T \\ -\boldsymbol{\alpha}^T & \mathbf{0}_n^T \\ \mathbf{0}_n^T & -\boldsymbol{\beta}^T \end{bmatrix} \begin{bmatrix} \boldsymbol{\lambda}_p \\ \boldsymbol{\lambda}_q \end{bmatrix} = \begin{bmatrix} -\left(\dfrac{\partial \boldsymbol{s}_{fl}}{\partial \boldsymbol{x}}\right)^T \boldsymbol{\mu} - \overline{\boldsymbol{\varphi}} + \underline{\boldsymbol{\varphi}} \\ -\lambda_{p_{ds}} \\ -\lambda_{q_{ds}} \end{bmatrix}$$

$$\implies \begin{bmatrix} \boldsymbol{\lambda}_p \\ \boldsymbol{\lambda}_q \end{bmatrix} = \left[\begin{bmatrix} \dfrac{\partial \boldsymbol{p}_f}{\partial \boldsymbol{x}} & -\boldsymbol{\alpha} & \mathbf{0}_n \\ \dfrac{\partial \boldsymbol{q}_f}{\partial \boldsymbol{x}} & \mathbf{0}_n & -\boldsymbol{\beta} \end{bmatrix}^{-1}\right]^T \begin{bmatrix} -\left(\dfrac{\partial \boldsymbol{s}_{fl}}{\partial \boldsymbol{x}}\right)^T \boldsymbol{\mu} - \overline{\boldsymbol{\varphi}} + \underline{\boldsymbol{\varphi}} \\ -\lambda_{p_{ds}} \\ -\lambda_{q_{ds}} \end{bmatrix}. \tag{67}$$

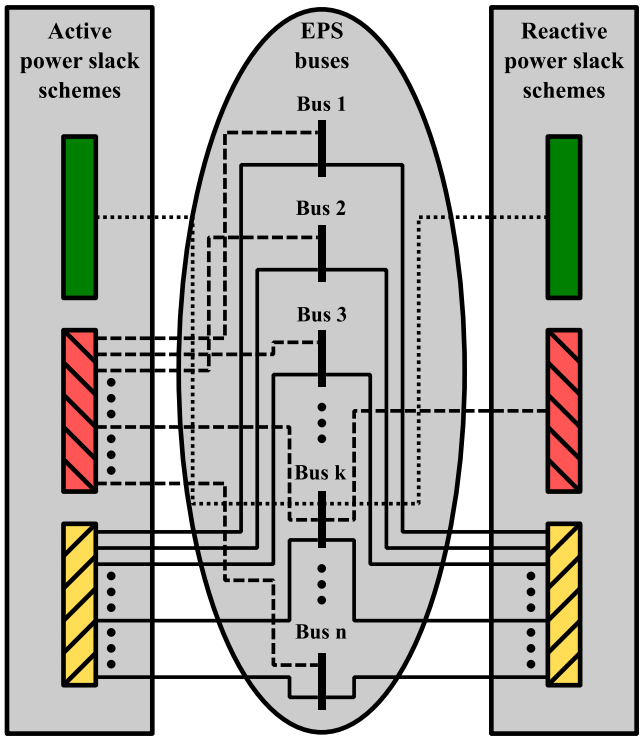

FIGURE 1. Diagram of different power compensation frameworks, where centralized compensation approaches are represented by single lines connected to a generic single slack bus k and distributed compensation approaches are represented by lines connected to all buses.

are calculated using (16), and the transmission reactive power losses are computed as follows:

$$q_l = \mathbf{1}_n^T \boldsymbol{q} + q_{ds}. \tag{73}$$

Differentiating (16) with respect to $\boldsymbol{q}$ and differentiating (73) with respect to $\boldsymbol{p}$ and $\boldsymbol{q}$ results in:

$$\frac{\partial p_l}{\partial \boldsymbol{q}} = \frac{\partial p_{ds}}{\partial \boldsymbol{q}} \tag{74}$$

$$\frac{\partial q_l}{\partial \boldsymbol{p}} = \frac{\partial q_{ds}}{\partial \boldsymbol{p}} \tag{75}$$

$$\frac{\partial q_l}{\partial \boldsymbol{q}} = \mathbf{1}_n + \frac{\partial q_{ds}}{\partial \boldsymbol{q}}. \tag{76}$$

Equations (17) and (74)–(76) can be combined to form the matrix composed of the active and reactive power loss sensitivity factors, as follows:

$$\begin{bmatrix} \frac{\partial p_{ds}}{\partial \boldsymbol{p}} & \frac{\partial q_{ds}}{\partial \boldsymbol{p}} \\ \frac{\partial p_{ds}}{\partial \boldsymbol{q}} & \frac{\partial q_{ds}}{\partial \boldsymbol{q}} \end{bmatrix} = \begin{bmatrix} -\mathbf{1}_n + \frac{\partial p_l}{\partial \boldsymbol{p}} & \frac{\partial q_l}{\partial \boldsymbol{p}} \\ \frac{\partial p_l}{\partial \boldsymbol{q}} & -\mathbf{1}_n + \frac{\partial q_l}{\partial \boldsymbol{q}} \end{bmatrix}. \tag{77}$$

Substituting (77) into (72) results in

$$\begin{bmatrix} \boldsymbol{\lambda}_p \\ \boldsymbol{\lambda}_q \end{bmatrix} = \begin{bmatrix} \mathbf{1}_n - \frac{\partial p_l}{\partial \boldsymbol{p}} & -\frac{\partial q_l}{\partial \boldsymbol{p}} \\ -\frac{\partial p_l}{\partial \boldsymbol{q}} & \mathbf{1}_n - \frac{\partial q_l}{\partial \boldsymbol{q}} \end{bmatrix} \begin{bmatrix} \lambda_{p_{ds}} \\ \lambda_{q_{ds}} \end{bmatrix} - \begin{bmatrix} \left(\frac{\partial \boldsymbol{s}_{fl}}{\partial \boldsymbol{p}}\right)^T \\ \left(\frac{\partial \boldsymbol{s}_{fl}}{\partial \boldsymbol{q}}\right)^T \end{bmatrix} \boldsymbol{\mu} - \begin{bmatrix} \left(\frac{\partial \boldsymbol{x}}{\partial \boldsymbol{p}}\right)^T \\ \left(\frac{\partial \boldsymbol{x}}{\partial \boldsymbol{q}}\right)^T \end{bmatrix} \left[\overline{\boldsymbol{\varphi}} - \underline{\boldsymbol{\varphi}}\right]. \tag{78}$$

Finally, from (78), the active power LMPs can be decomposed as follows:

$$\boldsymbol{\lambda}_p = \underbrace{\mathbf{1}_n \lambda_{p_{ds}}}_{\boldsymbol{\lambda}_p^e} \underbrace{- \frac{\partial p_l}{\partial \boldsymbol{p}} \lambda_{p_{ds}}}_{\boldsymbol{\lambda}_p^{pl}} \underbrace{- \frac{\partial q_l}{\partial \boldsymbol{p}} \lambda_{q_{ds}}}_{\boldsymbol{\lambda}_p^{ql}} \underbrace{- \left(\frac{\partial \boldsymbol{s}_{fl}}{\partial \boldsymbol{p}}\right)^T \boldsymbol{\mu}}_{\boldsymbol{\lambda}_p^c} \underbrace{- \left(\frac{\partial \boldsymbol{x}}{\partial \boldsymbol{p}}\right)^T \left[\overline{\boldsymbol{\varphi}} - \underline{\boldsymbol{\varphi}}\right]}_{\boldsymbol{\lambda}_p^x}. \tag{79}$$

$$\begin{aligned} \begin{bmatrix} \boldsymbol{\lambda}_p \\ \boldsymbol{\lambda}_q \end{bmatrix} &= \begin{bmatrix} \left(\frac{\partial \boldsymbol{x}}{\partial \boldsymbol{p}}\right)^T & \frac{\partial p_{ds}}{\partial \boldsymbol{p}} & \frac{\partial q_{ds}}{\partial \boldsymbol{p}} \\ \left(\frac{\partial \boldsymbol{x}}{\partial \boldsymbol{q}}\right)^T & \frac{\partial p_{ds}}{\partial \boldsymbol{q}} & \frac{\partial q_{ds}}{\partial \boldsymbol{q}} \end{bmatrix} \begin{bmatrix} -\left(\frac{\partial \boldsymbol{s}_{fl}}{\partial \boldsymbol{x}}\right)^T \boldsymbol{\mu} - \overline{\boldsymbol{\varphi}} + \underline{\boldsymbol{\varphi}} \\ -\lambda_{p_{ds}} \\ -\lambda_{q_{ds}} \end{bmatrix} \\ &= -\begin{bmatrix} \frac{\partial p_{ds}}{\partial \boldsymbol{p}} & \frac{\partial q_{ds}}{\partial \boldsymbol{p}} \\ \frac{\partial p_{ds}}{\partial \boldsymbol{q}} & \frac{\partial q_{ds}}{\partial \boldsymbol{q}} \end{bmatrix} \begin{bmatrix} \lambda_{p_{ds}} \\ \lambda_{q_{ds}} \end{bmatrix} + \begin{bmatrix} \left(\frac{\partial \boldsymbol{x}}{\partial \boldsymbol{p}}\right)^T \\ \left(\frac{\partial \boldsymbol{x}}{\partial \boldsymbol{q}}\right)^T \end{bmatrix} \left[-\left(\frac{\partial \boldsymbol{s}_{fl}}{\partial \boldsymbol{x}}\right)^T \boldsymbol{\mu} - \overline{\boldsymbol{\varphi}} + \underline{\boldsymbol{\varphi}}\right] \\ &= -\begin{bmatrix} \frac{\partial p_{ds}}{\partial \boldsymbol{p}} & \frac{\partial q_{ds}}{\partial \boldsymbol{p}} \\ \frac{\partial p_{ds}}{\partial \boldsymbol{q}} & \frac{\partial q_{ds}}{\partial \boldsymbol{q}} \end{bmatrix} \begin{bmatrix} \lambda_{p_{ds}} \\ \lambda_{q_{ds}} \end{bmatrix} - \begin{bmatrix} \left(\frac{\partial \boldsymbol{s}_{fl}}{\partial \boldsymbol{p}}\right)^T \\ \left(\frac{\partial \boldsymbol{s}_{fl}}{\partial \boldsymbol{q}}\right)^T \end{bmatrix} \boldsymbol{\mu} - \begin{bmatrix} \left(\frac{\partial \boldsymbol{x}}{\partial \boldsymbol{p}}\right)^T \\ \left(\frac{\partial \boldsymbol{x}}{\partial \boldsymbol{q}}\right)^T \end{bmatrix} \left[\overline{\boldsymbol{\varphi}} - \underline{\boldsymbol{\varphi}}\right]. \end{aligned} \tag{72}$$

Therefore, (79) provides the five LMP components from the decomposition model based on the traditional active power distributed slack approach and the proposed reactive power distributed slack scheme. The proposed decomposition model overcomes the inadequate point-to-point bidirectional relationship between active power increment and reactive power compensation in the context of LMP reactive power loss components of conventional decomposition approaches described in Section I.

In the new decomposition approach, the reactive power loss component of the LMP related to a specific bus is the marginal cost of reactive power losses when the source of the active power increment is situated on this bus, and the reactive power compensation is distributed across the EPS buses. This distributed reactive power compensation follows the proportion defined by the participation factors that constitute the vector $\boldsymbol{\beta}$. Thus, the proposed decomposition model provides a more adequate reactive power compensation framework, as it expands the range of possibilities for reactive energy reference specifications capable of harmonizing the interests of market participants.

There are several methodological possibilities through which participation factors constituting vector $\boldsymbol{\beta}$ can be calculated. Only three distinct approaches are presented, whose formulations represent the adaptation of the active power participation factor specification strategies in [37] for the reactive power instance. More sophisticated policies to obtain such factors are beyond the scope of this paper.

The first reactive energy reference specification policy is defined as:

$$\beta_i = \begin{cases} 1, & \forall i \in S \\ 0, & \forall i \notin S \end{cases} \tag{80}$$

where S is the unit set containing the single slack bus index.

In the participation factor specification model presented in (80), the reactive power output of a single generator is adjusted to achieve the reactive power balance of an EPS. Evidently, this policy corresponds to the conventional reactive power compensation scheme employed in decomposition models that consider the impact of reactive power on active power LMPs, as discussed in Section I.

The second reactive energy reference specification policy is given by:

$$\beta_i = \frac{q_{g,i}}{\mathbf{1}_n^T \boldsymbol{q}_g}, \quad \forall i \in N \tag{81}$$

where N is the set formed by the indices of all buses and $q_{g,i}$ is the *ith* element of the vector $\boldsymbol{q}_g$.

Essentially, in the participation factor computation strategy proposed in (81), the reactive power outputs of all generators are adjusted to enable the reactive power balance of an EPS, respecting the injection proportion defined by the participation factors.

Finally, the third reactive energy reference specification policy is governed by the following relationship:

$$\beta_i = \frac{q_{d,i}}{\mathbf{1}_n^T \boldsymbol{q}_d}, \quad \forall i \in N. \tag{82}$$

where $q_{d,i}$ is the *ith* element of the vector $\boldsymbol{q}_d$.

In the participation factor calculation scheme defined in (82), the reactive power balance of an EPS is achieved by distributing the reactive power mismatch between all the buses that have reactive loads.

IV. SIMULATION RESULTS

In this section, the financial impacts of the proposed decomposition model are presented and analyzed through simulations performed on the IEEE 30-bus test system. Unless otherwise noted, the network data of the IEEE 30-bus test system follow what is defined in [38], and the generation data follow what is proposed in [39]. The conventional and proposed decomposition models are implemented in MATLAB.

A. COMPARISON BETWEEN DECOMPOSITION MODELS

To explain further constraint modifications considered in the context of the IEEE 30-bus test system, the voltage limits defined in [40] are initially adopted. It is assumed that the conventional and proposed LMP decomposition models employ the load power adjustment variation defined in [37] as the active energy reference specification scheme. Furthermore, the proposed LMP decomposition approach adopts the reactive energy reference specification model described in (82). Initially, the LMPs and their components are calculated using the decomposition model proposed in Section III. From this computation, it is possible to verify that the state constraint components in $\boldsymbol{\lambda}_p^x$, in terms of absolute values, significantly prevail over $\boldsymbol{\lambda}_p^{pl}$, $\boldsymbol{\lambda}_p^{ql}$, and $\boldsymbol{\lambda}_p^c$. For example, in terms of absolute value, the state constraint component represents 95.5372% of the LMP at bus 1. LMP decomposition policies are fundamental to the implementation of risk hedging instruments in LMP-based markets. The most consolidated hedging tools in terms of practical applications are the FTRs, whose implementation is based on LMP congestion components. Some works consider that the LMP state constraint component derived in this paper is part of the LMP congestion component, as observed in [23]. However, this paper focuses on LMP congestion components that are purely associated with transmission power flow constraints. Because the essential purpose of the simulations performed in this paper is to assess the impact of the proposed decomposition model on financial settlements related to transmission congestion, such as in FTRs, a slight increase in voltage limits is considered. The lower and upper bus voltage limits are assumed to be 0.9 p.u. and 1.1 p.u., respectively. These new voltage limits are adopted in the simulations associated with the current comparison between decomposition models and in the simulations performed in Section IV-B. Such modifications are necessary for two reasons. First, to avoid the suspicion that

the voltage magnitude constraints are conveniently specified in order to purposely provide large discrepancies between the results arising from the conventional decomposition approach of Section II-A and the proposed decomposition model of Section III. Second, to focus research efforts on analyzing the impact of the proposed decomposition scheme on congestion pricing via differences between the components of vector $\boldsymbol{\lambda}_p^c$. Given the new voltage limits, the application of the proposed decomposition model produces LMP state constraint components and LMP congestion components equal to zero, which is expected.

It is essential to emphasize that it is absolutely expected that the application of different LMP decomposition models in the context of the same test system will produce different values for the LMPs and their respective components. The simulations performed in this section are not intended to corroborate the superiority of one model over another in terms of pricing magnitude. A model capable of providing lower LMPs is not necessarily better than one that provides higher LMPs. The main purpose of the comparison between decomposition approaches carried out in this section is to contextualize the decomposition model proposed in Section III with respect to referential results from a conventional decomposition scheme, such as that described in Section II-A. A feasible modification is made in the transmission limit of only one of the test system branches to contextualize the differences between the LMP components arising from the conventional decomposition strategy and the proposed decomposition model. The transmission limit of the branch between buses 6 and 28 is reduced from 32 MVA to 13 MVA. In view of the changes, LMPs and their components produced by the conventional and proposed decomposition models are shown in Table 1. Fig. 2 is included to highlight the spatial profile of LMPs produced by the conventional and proposed decomposition models. The total operating costs associated with the application of the conventional and proposed decomposition approaches are 570.9775 \$/h and 510.0407 \$/h, respectively.

In addition to contextualization, the comparisons made in this section also aim to introduce the metrics used to improve financial investigations of LMP congestion components from different decomposition cases. The metrics used to measure the disparity between LMP congestion components are defined as follows:

$$\delta_{i,j}^{k} = \begin{cases} \lambda_{p,i}^{c,k} - \lambda_{p,j}^{c,k}, & i \neq j \\ 0, & i = j \end{cases} \tag{83}$$

$$\Delta_{i,j}^{k,m} = \begin{cases} \delta_{i,j}^{k} - \delta_{i,j}^{m}, & i \neq j \\ 0, & i = j \end{cases} \tag{84}$$

$$\Delta_{i,j}^{k\longrightarrow m} = \begin{cases} -100\dfrac{\Delta_{i,j}^{k,m}}{\left|\delta_{i,j}^{k}\right|}, & (i \neq j) \wedge \left(\delta_{i,j}^{k} \neq 0\right) \\ 0, & (i = j) \wedge \left(\delta_{i,j}^{k} \neq 0\right) \\ \Psi, & \left(\delta_{i,j}^{k} = 0\right) \end{cases} \tag{85}$$

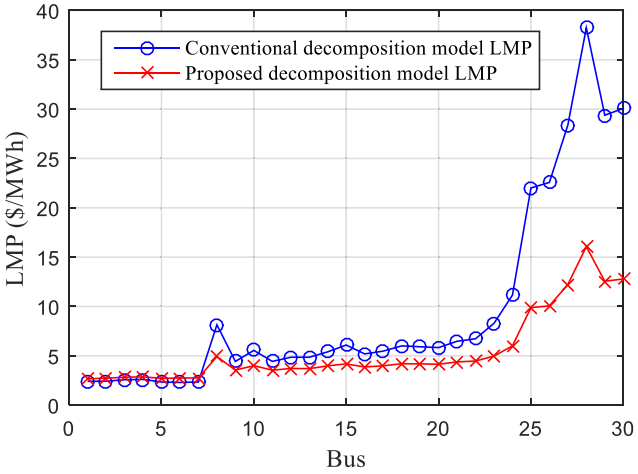

FIGURE 2. LMPs produced by the conventional (Case 1) and proposed (Case 2) decomposition models in the comparative investigation scenario.

$$\overline{\Delta^{k,m}} = \max\left(\boldsymbol{\Delta}^{k,m}\right) \tag{86}$$

$$\overline{\Delta^{k\longrightarrow m}} = \max\left(\boldsymbol{\Delta}^{k\longrightarrow m}\right) \tag{87}$$

where $\delta_{i,j}^{k}$ denotes the difference between congestion components (DCC) verified in the LMPs associated with buses i and j of an EPS within the scope of the decomposition results of a specific Case k. The scalars $\lambda_{p,i}^{c,k}$ and $\lambda_{p,j}^{c,k}$ represent the *ith* and *jth* elements of vector $\boldsymbol{\lambda}_p^c$ in a specific Case k, respectively. Parameter $\Delta_{i,j}^{k,m}$ is the nominal divergence between cases (NDC) and corresponds to the difference between the DCCs of buses i and j associated with a Case k and those related to a Case m. Parameter $\Delta_{i,j}^{k\longrightarrow m}$ is the percentage divergence between cases (PDC) and represents the percentage variation of DCC $\delta_{i,j}^{m}$ in relation to DCC $\delta_{i,j}^{k}$. Thus, the divergence PDC indicates the extent to which the differences between LMP congestion components vary in the transition between two cases under study. It is important to emphasize that the direction of this transition is relevant, since $\Delta_{i,j}^{k\longrightarrow m}$ can be significantly different from $\Delta_{i,j}^{m\longrightarrow k}$ in many scenarios, as they can be associated with very different comparative bases $\left|\delta_{i,j}^{k}\right|$ and $\left|\delta_{i,j}^{m}\right|$, respectively. The parameters $\overline{\Delta^{k,m}}$ and $\overline{\Delta^{k\longrightarrow m}}$ represent the maximum nominal divergence between cases (MNDC) and the maximum percentage divergence between cases (MPDC), respectively. The $n \times n$ matrix $\boldsymbol{\Delta}^{k,m}$ is formed by all possible NDCs related to the decomposition results for Cases k and m. The $n \times n$ matrix $\boldsymbol{\Delta}^{k\longrightarrow m}$ is composed of all possible PDCs related to the transition of the decomposition results from a Case k to a Case m. The scalars $\Delta_{i,j}^{k,m}$ and $\Delta_{i,j}^{k\longrightarrow m}$ calculated in (84) and (85) represent the elements located in the *ith* row and *jth* column of matrices $\boldsymbol{\Delta}^{k,m}$ and $\boldsymbol{\Delta}^{k\longrightarrow m}$, respectively. It is possible to notice that the matrices $\boldsymbol{\Delta}^{k,m}$ and $\boldsymbol{\Delta}^{k\longrightarrow m}$ are antisymmetric. The scalar Ψ is a large number conveniently chosen to indicate that it represents the condition of largest possible percentage variation, that is, the percentage variation

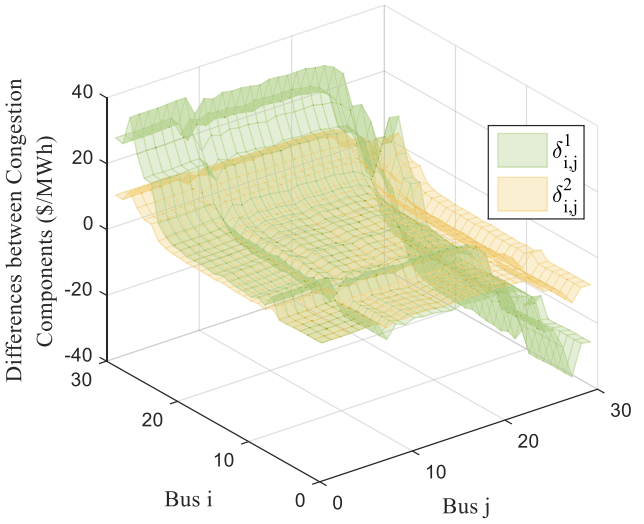

FIGURE 3. DCCs produced by the conventional (Case 1) and proposed (Case 2) decomposition models in the comparative investigation scenario.

of DCC $\delta^m_{i,j}$ in relation to DCC $\delta^k_{i,j}$, when $\left|\delta^k_{i,j}\right| = 0$. In the simulations performed in this section and in Section IV-B, there is no need to define values for Ψ, because $\left|\delta^k_{i,j}\right| \neq 0$ for all Cases k and $\forall i, j \in N$. The operator max $(\boldsymbol{A})$ identifies the largest element in the matrix $\boldsymbol{A}$.

In the current study, Case 1 corresponds to the application of the conventional decomposition approach described in Section II-A, and Case 2 represents the use of the decomposition model proposed in Section III. To expose the general context of the comparison between the LMP congestion components provided in Cases 1 and 2, all DCCs from such cases are illustrated in Fig. 3. Furthermore, all NDCs provided in Cases 1 and 2 are shown in Fig. 4. Using (86) and (87), the MNDC and MPDCs associated with the results from the decomposition scenarios defined in Cases 1 and 2 are calculated as follows:

$$\overline{\Delta^{1,2}} = \max\left(\boldsymbol{\Delta}^{1,2}\right) = \Delta^{1,2}_{28,6} = 22.6056\ \$/\text{MWh}$$
$$\overline{\Delta^{1\longrightarrow 2}} = \max\left(\boldsymbol{\Delta}^{1\longrightarrow 2}\right) = \Delta^{1\longrightarrow 2}_{13,12} = -2.4461 \times 10^7\%$$
$$\overline{\Delta^{2\longrightarrow 1}} = \max\left(\boldsymbol{\Delta}^{2\longrightarrow 1}\right) = \Delta^{2\longrightarrow 1}_{3,2} = -1780.0499\%$$

First, it is possible to observe that the MPDCs were calculated for Case 1 to Case 2 and for Case 2 to Case 1, because, as mentioned before, the transition direction between cases can significantly affect the MPDC calculation. MNDC $\overline{\Delta^{1,2}} = \Delta^{1,2}_{28,6} = 22.6056\ \$/\text{MWh}$ represents the potential financial difference between possible congestion pricing schemes associated with the decomposition models described in Sections II-A and III if the buses involved in the transactions are 6 and 28. In the specific LMP scenario produced by the two decomposition models applied in the IEEE 30-bus test system, the value 22.6056 $/MWh is significant. More specifically, this amount indicates that if a congestion pricing policy switches from the decomposition

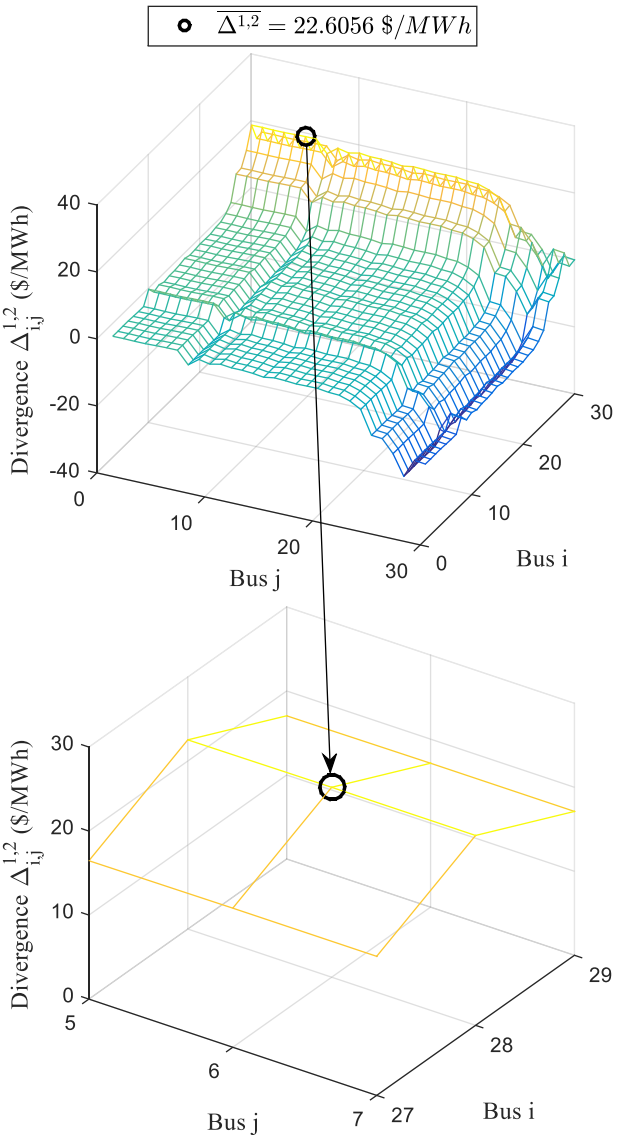

FIGURE 4. NDCs regarding the conventional (Case 1) and proposed (Case 2) decomposition models in the comparative investigation scenario.

approach defined in Case 1 to that used in Case 2, participants who settle transactions based on the difference between the LMP congestion components of buses 28 and 6 will see a -62.9919% variation in the corresponding DCC, i.e., $\Delta^{1\longrightarrow 2}_{28,6} = -62.9919\%$. These transaction settlements may represent, for example, congestion charges for bilateral transactions in day-ahead markets [41], application of FTRs in hedging schemes, or other electricity market financial settlement frameworks addressed in future research. Analogously, if a congestion pricing policy changes from the decomposition model defined in Case 2 to the one used in Case 1, participants who settle transactions based on the difference between the LMP congestion components of buses 28 and 6 will see a 170.2112% variation in the correlated DCC, that is, $\Delta^{2\longrightarrow 1}_{28,6} = 170.2112\%$. MPDC $\overline{\Delta^{1\longrightarrow 2}} = \Delta^{1\longrightarrow 2}_{13,12} = -2.4461 \times 10^7\%$ indicates the potential financial

TABLE 1. LMPs and their components produced by the conventional (Case 1) and proposed (Case 2) decomposition models in the comparative investigation scenario.

Bus	Conventional LMP decomposition model (Case 1)			Proposed LMP decomposition model (Case 2)				
	λ_p^e (\$/MWh)			λ_p^e (\$/MWh)				
	7.4380			4.6503				
	λ_p (\$/MWh)	λ_p^{pl} (\$/MWh)	λ_p^c (\$/MWh)	λ_p (\$/MWh)	λ_p^{pl} (\$/MWh)	λ_p^{ql} (\$/MWh)	λ_p^c (\$/MWh)	λ_p^x (\$/MWh)
1	2.4192	-0.3290	-4.6898	2.6788	-0.2699	-0.0615	-1.6401	0.0000
2	2.4230	-0.2261	-4.7889	2.7262	-0.1745	-0.0453	-1.7043	0.0000
3	2.5778	-0.1437	-4.7165	2.8342	-0.0847	-0.0309	-1.7004	0.0000
4	2.6094	-0.1100	-4.7186	2.8646	-0.0499	-0.0250	-1.7108	0.0000
5	2.3488	-0.2053	-4.8839	2.7169	-0.1376	-0.0360	-1.7597	0.0000
6	2.3024	-0.0742	-5.0613	2.7492	-0.0267	-0.0212	-1.8531	0.0000
7	2.3450	-0.0497	-5.0433	2.7621	-0.0272	-0.0219	-1.8390	0.0000
8	8.1443	-0.0740	0.7803	4.9249	-0.0267	-0.0213	0.3227	0.0000
9	4.4346	-0.0565	-2.9469	3.5581	-0.0237	-0.0012	-1.0673	0.0000
10	5.5522	-0.0473	-1.8386	4.0042	-0.0216	0.0148	-0.6393	0.0000
11	4.4346	-0.0565	-2.9469	3.5444	-0.0233	-0.0098	-1.0727	0.0000
12	4.8558	-0.1855	-2.3967	3.7189	-0.0692	0.0087	-0.8709	0.0000
13	4.8558	-0.1855	-2.3967	3.7046	-0.0671	0.0011	-0.8796	0.0000
14	5.4026	-0.0396	-1.9958	3.9806	0.0088	0.0179	-0.6963	0.0000
15	6.0964	0.0491	-1.3907	4.1832	0.0347	0.0194	-0.5211	0.0000
16	5.1949	-0.0703	-2.1728	3.8700	-0.0215	0.0146	-0.7734	0.0000
17	5.4740	-0.0193	-1.9447	3.9862	-0.0031	0.0172	-0.6781	0.0000
18	6.0058	0.1482	-1.5804	4.1988	0.0844	0.0256	-0.5614	0.0000
19	5.9203	0.1640	-1.6817	4.1850	0.0929	0.0273	-0.5854	0.0000
20	5.8344	0.1197	-1.7233	4.1449	0.0687	0.0247	-0.5988	0.0000
21	6.4725	0.0391	-1.0046	4.3808	0.0259	0.0205	-0.3160	0.0000
22	6.7272	0.0369	-0.7477	4.4741	0.0249	0.0204	-0.2216	0.0000
23	8.2902	0.1437	0.7085	4.9700	0.0788	0.0242	0.2167	0.0000
24	11.1529	0.1864	3.5285	6.0077	0.0963	0.0265	1.2346	0.0000
25	22.0084	0.1411	14.4293	9.8821	0.0662	0.0245	5.1412	0.0000
26	22.5710	0.3348	14.7981	10.0651	0.1617	0.0325	5.2207	0.0000
27	28.3817	0.0372	20.9065	12.2347	0.0077	0.0190	7.5577	0.0000
28	38.2370	-0.0261	30.8251	16.0609	0.0000	-0.0172	11.4278	0.0000
29	29.3854	0.3015	21.6459	12.5617	0.1521	0.0340	7.7253	0.0000
30	30.0669	0.4810	22.1479	12.7899	0.2525	0.0442	7.8428	0.0000

percentage difference between possible congestion pricing approaches based on the decomposition schemes defined in Sections II-A and III if the buses involved in the transactions are 12 and 13. This percentage indicates that if a congestion pricing scheme changes from the decomposition model used in Case 1 to that used in Case 2, participants who settle transactions based on the difference between the LMP congestion components of buses 13 and 12 will see their DCCs vary from $\delta^1_{13,12} = -3.5698 \times 10^{-8}$ to $\delta^2_{13,12} = -0.0087$, that is, $\Delta^{1,2}_{13,12} = 0.0087$. These values show how financial studies based solely on percentage changes can be misleading, as the MPDC $\overline{\Delta^{1\longrightarrow 2}} = -2.4461 \times 10^7\%$ only has this large magnitude due to the very small base value $\delta^1_{13,12} = -3.5698 \times 10^{-8}$ against which the percentage decrease is computed. This highlights the need for studies of this type to consider nominal and percentage variations simultaneously, considering the purposes of the investigations. MPDC $\overline{\Delta^{2\longrightarrow 1}} = \Delta^{2\longrightarrow 1}_{3,2} = -1780.0499\%$ can be analyzed in a similar manner.

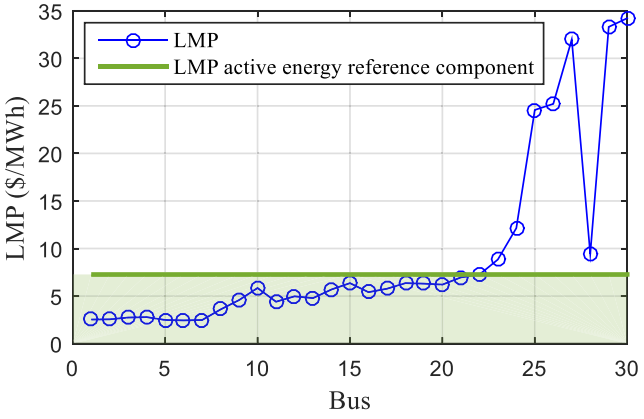

FIGURE 5. LMPs and LMP active energy reference component produced by the proposed decomposition model in all cases considered in the investigation scenario concerning reactive energy reference impacts.

B. REACTIVE ENERGY REFERENCE IMPACTS

This section highlights the relevance of the disparity between LMP components arising solely from the application of

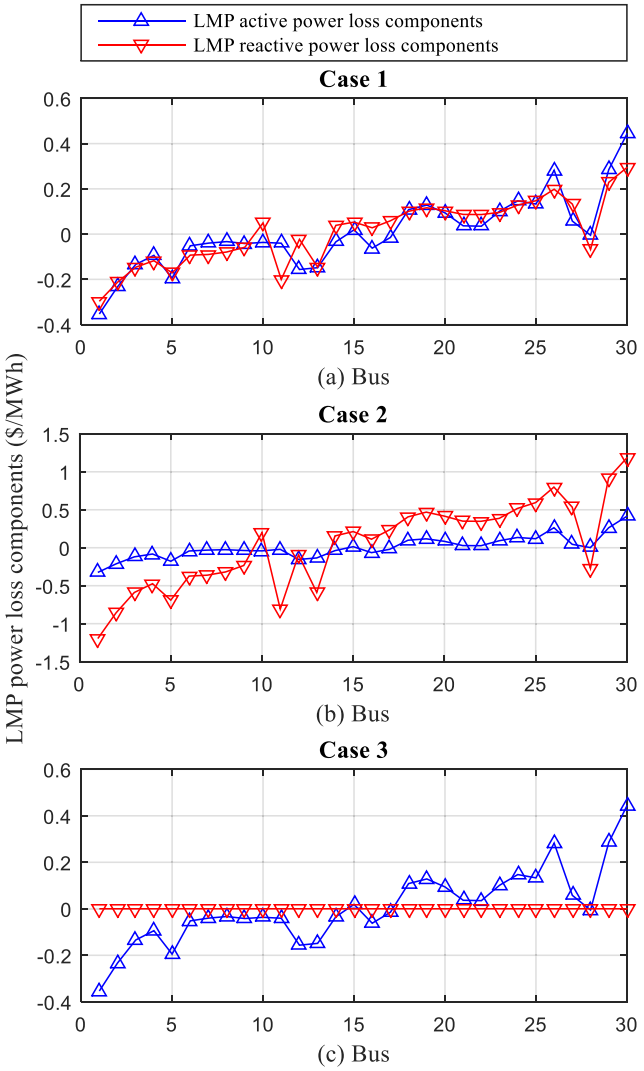

FIGURE 6. LMP active and reactive power loss components produced by the proposed decomposition model in (a) Case 1, (b) Case 2, and (c) Case 3 considered in the investigation scenario concerning reactive energy reference impacts.

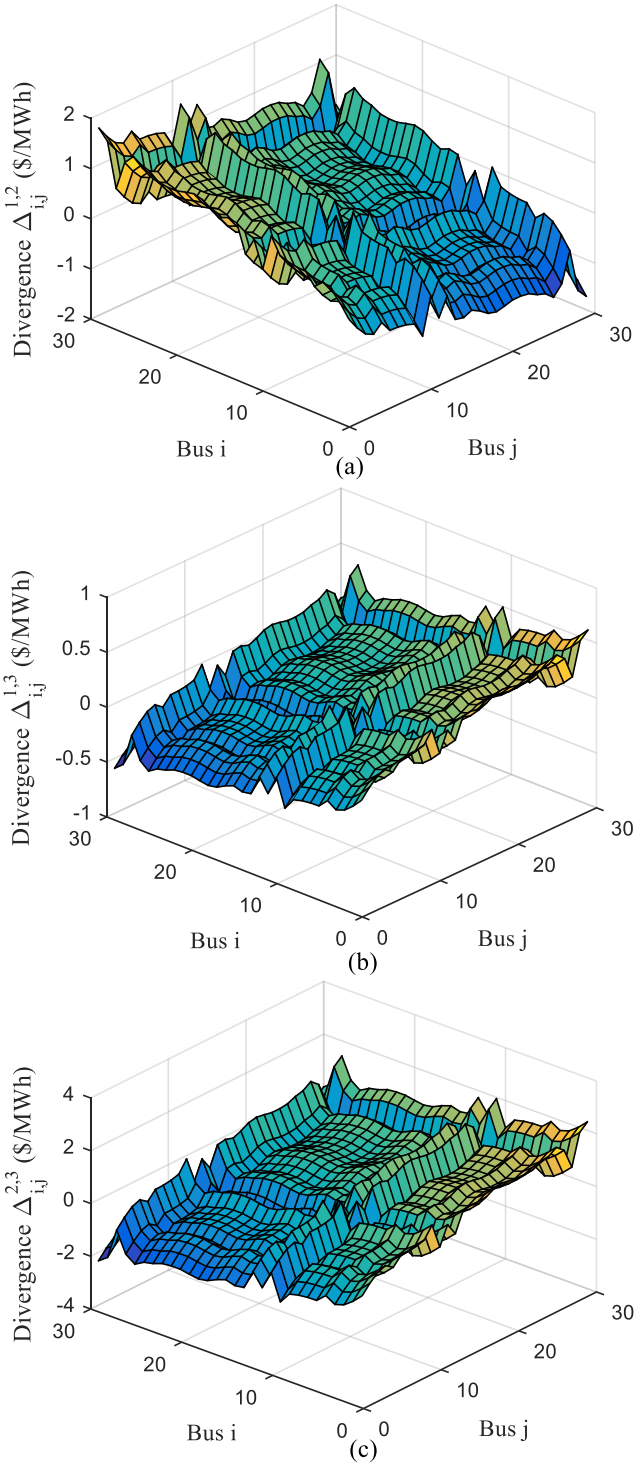

FIGURE 7. NDCs produced by the proposed decomposition model considering (a) Cases 1 and 2, (b) Cases 1 and 3, and (c) Cases 2 and 3 used in the investigation scenario concerning reactive energy reference impact.

the proposed decomposition model under different reactive energy reference specifications. It is demonstrated that the LMP components calculated using the proposed decomposition model vary significantly in the face of changes in the reactive energy reference specifications, even when the active energy reference is unchanged and the test system conditions are unaltered. The LMP values remain unchanged, whereas their components vary considerably with different reactive energy reference selections.

For the simulations in this section, the transmission limits of the branch between buses 6 and 28, and the branch between buses 28 and 27 are reduced from 32 to 13 MVA and from 65 to 16 MVA, respectively. Three distinct cases are considered in the current study. In Case 1, the reactive energy reference specification follows that defined in (82). In Case 2, the reactive energy reference specification is based on the attribution of a unitary participation factor to the bus with the highest reactive power LMP and zero participation factors to the other buses. More specifically, $\beta_{30} = 1$ and $\beta_i = 0, \forall i \in \{1, 2, \ldots, 30\} - \{30\}$. In Case 3, the reactive energy reference specification is based on the attribution of a unitary participation factor to the bus with the lowest reactive power LMP

FIGURE 8. Ranking and related metrics of (a) largest NDCs associated with Cases 1 and 2, (b) largest PDCs from Case 1 to Case 2, and (c) largest PDCs from Case 2 to Case 1.

and zero participation factors to the other buses. Basically, $\beta_2 = 1$ and $\beta_i = 0, \forall i \in \{1, 2, \ldots, 30\} - \{2\}$. Again, it is assumed that the proposed decomposition model employs the load power adjustment variation derived in [37] as the active energy reference specification approach. The LMPs and their active energy reference components produced by applying the proposed decomposition model to Cases 1, 2, and 3 are shown in Fig. 5. In order to demonstrate the significance of the LMP reactive power loss components produced by the proposed decomposition approach, the active power loss and reactive power loss components associated with each case are illustrated in Fig. 6. The total operating cost associated with applying the proposed decomposition model is 550.5286 $/h.

To illustrate the general context of the comparison between the LMP congestion components provided in Cases 1 and 2, between the components provided in Cases 1 and 3, and between the components provided in Cases 2 and 3, all DCCs associated with such pairs of cases are shown in Fig. 7. To more accurately examine the disparity between the LMP congestion components from the different decomposition scenarios defined in Cases 1, 2, and 3, the divergence metrics NDC and PDC are presented in descending order ranking arrangements. Fig. 8a presents the 20 largest NDCs in

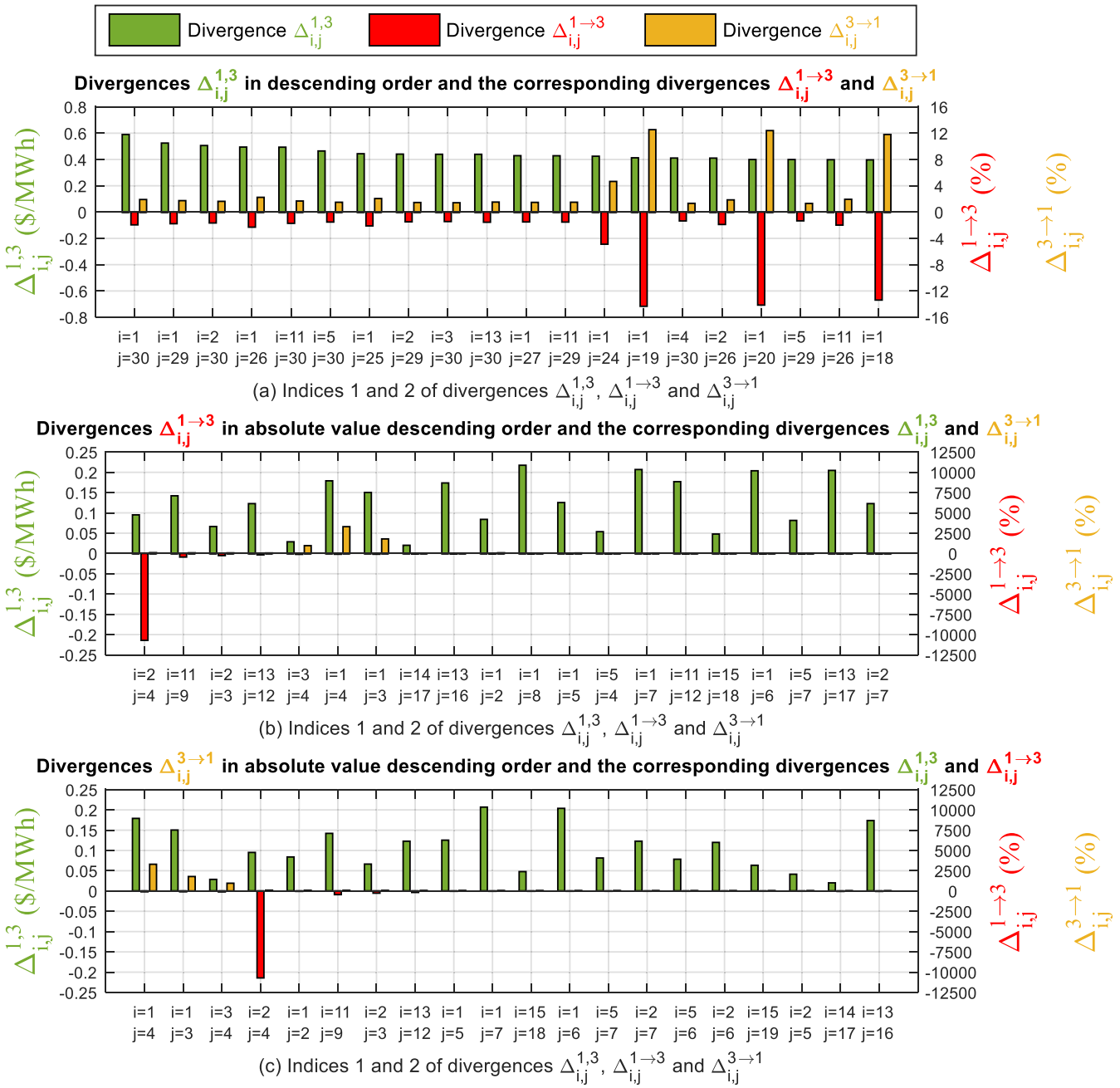

FIGURE 9. Ranking and related metrics of (a) largest NDCs associated with Cases 1 and 3, (b) largest PDCs from Case 1 to Case 3, and (c) largest PDCs from Case 3 to Case 1.

descending order associated with Cases 1 and 2. The PDCs in both case directions (Case 1 to Case 2 and Case 2 to Case 1) corresponding to these NDCs are also illustrated in Fig. 8a. The 20 largest PDCs from Case 1 to Case 2, in descending order in terms of absolute values, are shown in Fig. 8b. The corresponding NDCs and PDCs from Case 2 to Case 1 are shown in Fig. 8b. The 20 largest PDCs from Case 2 to Case 1, in descending order in terms of absolute values, are illustrated in Fig. 8c. The corresponding NDCs and PDCs from Case 1 to Case 2 are illustrated in Fig. 8c. If the same logic of formulating descending order ranking arrangements is followed for the comparison between Cases 1 and 3, and for the comparison between Cases 2 and 3, Figs. 9 and 10 are obtained, respectively.

Regarding the comparison between Cases 1 and 2, it is obvious that the MNDC is equivalent to the first NDC of the ranking shown in Fig. 8a, that is, $\overline{\Delta^{1,2}} = \Delta^{1,2}_{30,1} = 1.7328$ \$/MWh. However, within the NDC ranking presented in Fig. 8a, the NDC that presents the highest PDC from Case 1 to Case 2 in terms of absolute value is the one in the 14th position, where $\Delta^{1,2}_{19,1} = 1.2122$ \$/MWh and $\Delta^{1\longrightarrow2}_{19,1} = -42.0834\%$. In the context of the same NDC ranking presented in Fig. 8a, the NDC that presents the highest PDC of Case 2 to Case 1 in terms of absolute value is also that

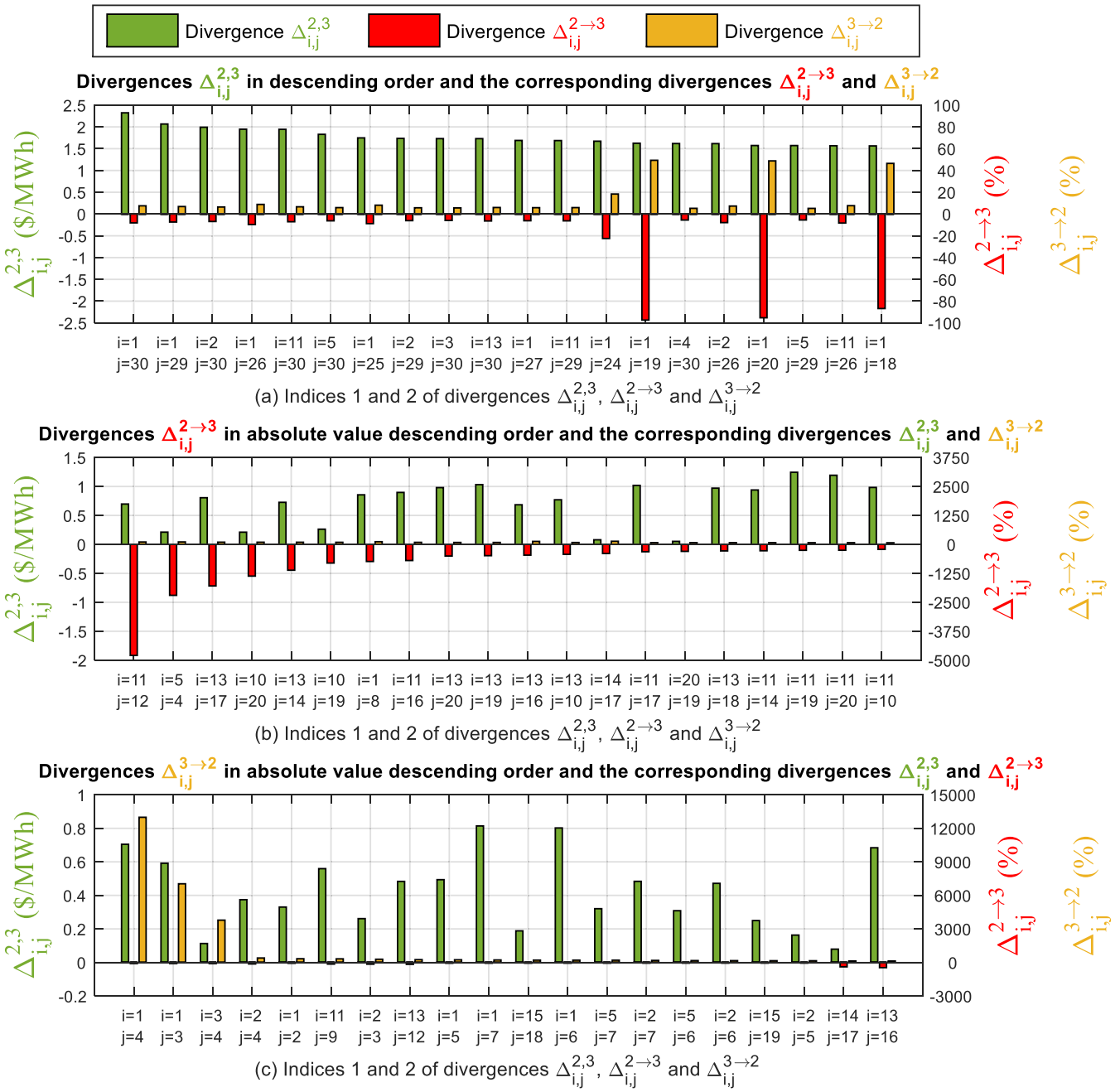

FIGURE 10. Ranking and related metrics of (a) largest NDCs associated with Cases 2 and 3, (b) largest PDCs from Case 2 to Case 3, and (c) largest PDCs from Case 3 to Case 2.

of the 14th position, where $\Delta^{2\longrightarrow1}_{19,1} = 72.6622\%$. Still in the comparison between Cases 1 and 2, it is clear that the MPDC from Case 1 to Case 2 is equivalent to the first PDC of the ranking illustrated in Fig. 8b, i.e., $\overline{\Delta^{1\longrightarrow2}} = \Delta^{1\longrightarrow2}_{4,2} = -3.1460 \times 10^4\%$. However, in the PDC ranking shown in Fig. 8b, the PDC from Case 1 towards Case 2 that has the highest NDC is that of the 11th position, where $\Delta^{1,2}_{8,1} = 0.6385$ \$/MWh and $\Delta^{1\longrightarrow2}_{8,1} = -122.1979\%$. Continuing in the comparison between Cases 1 and 2, it is evident that the MPDC from Case 2 to Case 1 is the first PDC of the ranking shown in Fig. 8c, i.e., $\overline{\Delta^{2\longrightarrow1}} = \Delta^{2\longrightarrow1}_{12,11} = 3.5762 \times 10^3\%$. However, in the PDC ranking shown in Fig. 8c, the PDC from case 2 towards case 1 that has the highest NDC is that of the 18th position, where $\Delta^{1,2}_{19,11} = 0.9293$ \$/MWh and $\Delta^{2\longrightarrow1}_{19,11} = 190.3559\%$. The same investigations can be readily extended to the comparison between Cases 1 and 3 and to the comparison between Cases 2 and 3 through Figs. 9 and 10, respectively.

The general scenarios of the MNDCs and MPDCs calculated for all possible combinations of the three cases are shown in Tables 2 and 3, respectively. From Table 2, the largest MNDC verified from the comparisons between all

the proposed decomposition cases is that associated with the comparison between Cases 2 and 3, that is, $\overline{\Delta^{2,3}} = \Delta^{2,3}_{1,30} = 2.3228$ \$/MWh. This value indicates the financial difference between the possible congestion pricing approaches associated with Cases 2 and 3 if the buses involved in the transactions are 1 and 30. This monetary quantity indicates a significant difference between the decomposition results from Cases 2 and 3, despite the adoption of the same LMP decomposition model. Essentially, this amount indicates that if a congestion pricing policy switches from the decomposition scheme defined in Case 2 to that used in Case 3, participants who settle transactions based on the difference between the LMP congestion components of buses 1 and 30 will see a -8.1300% variation in the corresponding DCC, i.e., $\Delta^{2\longrightarrow 3}_{1,30} = -8.1300\%$. Similarly, if a congestion pricing policy changes from the decomposition approach defined in Case 3 to that used in Case 2, participants who settle transactions governed by the difference between the LMP congestion components of buses 1 and 30 will see a 7.5188% variation in the correlated DCC, i.e., $\Delta^{3\longrightarrow 2}_{1,30} = 7.5188\%$.

TABLE 2. MNDCs calculated for all possible combinations between all cases considered in the investigation scenario concerning reactive energy reference impacts.

Cases	MNDC data		Corresponding PDC data	
	NDC that represents the MNDC	MNDC ($/MWh)	PDC corresponding to MNDC	PDC (%)
1 and 2	$\Delta^{1,2}_{30,1}$	1.7328	$\Delta^{1\rightarrow 2}_{30,1}$	-5.7183
			$\Delta^{2\rightarrow 1}_{30,1}$	6.0651
1 and 3	$\Delta^{1,3}_{1,30}$	0.5900	$\Delta^{1\rightarrow 3}_{1,30}$	-1.9469
			$\Delta^{3\rightarrow 1}_{1,30}$	1.9097
2 and 3	$\Delta^{2,3}_{1,30}$	2.3228	$\Delta^{2\rightarrow 3}_{1,30}$	-8.1300
			$\Delta^{3\rightarrow 2}_{1,30}$	7.5188

TABLE 3. MPDCs calculated for all possible combinations and directions between all cases considered in the investigation scenario concerning reactive energy reference impacts.

Cases	MPDC data		Corresponding NDC data	
	PDC that represents the MPDC	MPDC (%)	NDC corresponding to MPDC	NDC ($/MWh)
1 and 2	$\Delta^{1\rightarrow 2}_{4,2}$	-3.1460×10^{4}	$\Delta^{1,2}_{4,2}$	0.2793
	$\Delta^{2\rightarrow 1}_{12,11}$	3.5762×10^{3}	$\Delta^{1,2}_{12,11}$	0.5197
1 and 3	$\Delta^{1\rightarrow 3}_{2,4}$	-1.0711×10^{4}	$\Delta^{1,3}_{2,4}$	0.0951
	$\Delta^{3\rightarrow 1}_{1,4}$	3.2995×10^{3}	$\Delta^{1,3}_{1,4}$	0.1790
2 and 3	$\Delta^{2\rightarrow 3}_{11,12}$	-4.7937×10^{3}	$\Delta^{2,3}_{11,12}$	0.6967
	$\Delta^{3\rightarrow 2}_{1,4}$	1.2991×10^{4}	$\Delta^{2,3}_{1,4}$	0.7049

From Table 3, the largest MPDC observed from the comparisons between all the proposed decomposition cases is the one related to the comparison between Cases 1 and 2, considering Case 1 to Case 2, i.e., $\overline{\Delta^{1\longrightarrow 2}} = \Delta^{1\longrightarrow 2}_{4,2} = -3.1460\times10^{4}\%$. This value indicates the potential financial percentage difference between possible congestion pricing approaches based on the reactive power reference specifications of Cases 1 and 2 if the buses involved in the transactions are 4 and 2. This percentage indicates that if the proposed decomposition model changes the reactive power reference specification used in Case 1 to that used in Case 2, participants who settle transactions based on the difference between the LMP congestion components of buses 4 and 2 will see their parameters vary from $\delta^{1}_{4,2} = -8.8782\times10^{-4}$ to $\delta^{2}_{4,2} = -0.2802$, i.e., $\Delta^{1,2}_{4,2} = 0.2793$.

V. CONCLUSION

In this paper, an LMP decomposition model based on an OPF framework integrated with a fully distributed slack scheme is proposed. Modelling improvements to overcome the market inadequacies associated with power slack approaches that govern decomposition models have traditionally focused only on the active power scope. This incompleteness is overcome by incorporating a reactive power distributed slack bus model in the derivation of the LMP components. The inappropriate bilateral nature of conventional reactive power offsets that quantify LMP reactive power loss components is addressed by incorporating a multilateral compensation approach that involves any desired buses in any proportion. The proposed decomposition model conceives a pertinent source of negotiations between market participants, as it is now necessary to specify the reactive energy reference in parallel with the traditional active energy reference selection. The main purpose of LMP decomposition is the implementation of risk hedging instruments, mainly FTRs, which are significantly affected by the proposed decomposition model. Such impacts are measured using metrics that compute the magnitude of the financial disparity between the LMP congestion components calculated through simulations on a test system. These disparities are observed not only between the conventional and proposed decomposition approaches but also between different cases involving the application of the proposed decomposition model. In such cases, different reactive energy reference specifications are used, the active energy reference setting remains unchanged, and the test system conditions are preserved. Furthermore, in these cases, the results of applying the proposed decomposition model demonstrated the relevance of the reactive power loss components in the LMP composition.

REFERENCES

[1] F. C. Schweppe, M. C. Caramanis, R. D. Tabors, and R. E. Bohn, *Spot Pricing of Electricity*. Norwell, MA, USA: Kluwer, 1988.
[2] W. W. Hogan, "Contract networks for electric power transmission," *J. Regulatory Econ.*, vol. 4, no. 3, pp. 211–242, Sep. 1992.
[3] W. W. Hogan, "Financial transmission right formulations," John F. Kennedy Sch. Gov., Harvard Univ., Cambridge, MA, USA, Tech. Rep., 2002. [Online]. Available: https://scholar.harvard.edu/whogan/files/ftr_formulations_033102.pdf

[4] K. Xie, Y. H. Song, J. Stonham, E. Yu, and G. Liu, "Decomposition model and interior point methods for optimal spot pricing of electricity in deregulation environments," *IEEE Trans. Power Syst.*, vol. 15, no. 1, pp. 39–50, Feb. 2000.
[5] T. Wu, Z. Alaywan, and A. D. Papalexopoulos, "Locational marginal price calculations using the distributed-slack power-flow formulation," *IEEE Trans. Power Syst.*, vol. 20, no. 2, pp. 1188–1190, May 2005.
[6] T. Orfanogianni and G. Gross, "A general formulation for LMP evaluation," *IEEE Trans. Power Syst.*, vol. 22, no. 3, pp. 1163–1173, Aug. 2007.
[7] V. Sarkar and S. A. Khaparde, "Optimal LMP decomposition for the ACOPF calculation," *IEEE Trans. Power Syst.*, vol. 26, no. 3, pp. 1714–1723, Aug. 2011.
[8] F. O. S. Saraiva and V. L. Paucar, "General Metaheuristic-based methodology for computation and decomposition of LMPs," *Electr. Eng.*, vol. 103, no. 2, pp. 793–811, Apr. 2021.
[9] A. Castillo, P. Lipka, J.-P. Watson, S. S. Oren, and R. P. O'Neill, "A successive linear programming approach to solving the IV-ACOPF," *IEEE Trans. Power Syst.*, vol. 31, no. 4, pp. 2752–2763, Jul. 2016.
[10] H. Liu, L. Tesfatsion, and A. A. Chowdhury, "Locational marginal pricing basics for restructured wholesale power markets," in *Proc. IEEE Power Energy Soc. Gen. Meeting*, Calgary, AB, Canada, Jul. 2009, pp. 1–8.
[11] P. Lipka, S. S. Oren, R. P. O'neill, and A. Castillo, "Running a more complete market with the SLP-IV-ACOPF," *IEEE Trans. Power Syst.*, vol. 32, no. 2, pp. 1139–1148, Mar. 2017.
[12] F. L. Alvarado, "Converting system limits to market signals," *IEEE Trans. Power Syst.*, vol. 18, no. 2, pp. 422–427, May 2003.
[13] K. Abdul-Rahman, J. Wu, E. Haq, and P. Ristanovic, "Considerations of reactive power/voltage control in CAISO market operations," in *Proc. IEEE Power Energy Soc. Gen. Meeting*, Detroit, MI, USA, Jul. 2011, pp. 1–6.
[14] R. P. O'Neill, T. Dautel, and E. Krall, "Recent ISO software enhancements and future software and modeling plans," Fed. Energy Regul. Com., Washington, DC, USA, Staff Rep., Nov. 2011.
[15] *National Academies of Sciences, Engineering, and Medicine, Analytic Research Foundations for the Next-Generation Electric Grid*, Nat. Academies Press, Washington, DC, USA, 2016.
[16] *The Value of Economic Dispatch*, A Rep. Congr. Purs. Sect. 1234 Energy Policy Act 2005, United States Dept. Energy, Washington, DC, USA, Nov. 2005.
[17] M. Rivier and I. J. Pérez-Arriaga, "Computation and decomposition of spot prices for transmission pricing," in *Proc. 11th Power Syst. Comput. Conf.*, Avignon, France, 1993, pp. 371–378.
[18] A. A. El-Keib and X. Ma, "Calculating short-run marginal costs of active and reactive power production," *IEEE Trans. Power Syst.*, vol. 12, no. 2, pp. 559–565, May 1997.
[19] J. D. Finney, H. Othman, and W. L. Rutz, "Evaluating transmission congestion constraints in system planning," *IEEE Trans. Power Syst.*, vol. 12, no. 3, pp. 1143–1150, Aug. 1997.
[20] L. Chen, H. Suzuki, T. Wachi, and Y. Shimura, "Components of nodal prices for electric power systems," *IEEE Trans. Power Syst.*, vol. 17, no. 1, pp. 41–49, Feb. 2002.
[21] G. C. Stamtsis and I. Erlich, "Congestion analysis and participants' behaviour in a pool market," *IEE Proc.-Gener. Transm. Distrib.*, vol. 151, no. 1, pp. 127–131, Jan. 2004.
[22] E. Litvinov, T. Zheng, G. Rosenwald, and P. Shamsollahi, "Marginal loss modeling in LMP calculation," *IEEE Trans. Power Syst.*, vol. 19, no. 2, pp. 880–888, May 2004.
[23] X. Cheng and T. J. Overbye, "An energy reference bus independent LMP decomposition algorithm," *IEEE Trans. Power Syst.*, vol. 21, no. 3, pp. 1041–1049, Aug. 2006.
[24] J. B. Cardell, "Marginal loss pricing for hours with transmission congestion," *IEEE Trans. Power Syst.*, vol. 22, no. 4, pp. 1466–1474, Nov. 2007.
[25] F. Li and R. Bo, "DCOPF-based LMP simulation: Algorithm, comparison with ACOPF, and sensitivity," *IEEE Trans. Power Syst.*, vol. 22, no. 4, pp. 1475–1485, Nov. 2007.
[26] F. Li, "Continuous locational marginal pricing (CLMP)," *IEEE Trans. Power Syst.*, vol. 22, no. 4, pp. 1638–1646, Nov. 2007.
[27] L. Wang and M. Mazumdar, "Using a system model to decompose the effects of influential factors on locational marginal prices," *IEEE Trans. Power Syst.*, vol. 22, no. 4, pp. 1456–1465, Nov. 2007.
[28] C. Li, K. W. Hedman, and M. Zhang, "Market pricing with single-generator-failure security constraints," *IET Gener., Transmiss. Distrib.*, vol. 11, no. 7, pp. 1777–1785, May 2017.
[29] T. Vaskovskaya, P. G. Thakurta, and J. Bialek, "Contribution of transmission and voltage constraints to the formation of locational marginal prices," *Int. J. Electr. Power Energy Syst.*, vol. 101, pp. 491–499, Oct. 2018.
[30] M. Samadi and M. E. Hajiabadi, "Assessment of the collusion possibility and profitability in the electricity market: A new analytical approach," *Int. J. Electr. Power Energy Syst.*, vol. 112, pp. 381–392, Nov. 2019.
[31] M. J. P. Jaghargh and H. R. Mashhadi, "An analytical approach to estimate structural and behavioral impact of renewable energy power plants on LMP," *Renew. Energy*, vol. 163, pp. 1012–1022, Jan. 2021.
[32] S. Hanif, K. Zhang, C. M. Hackl, M. Barati, H. B. Gooi, and T. Hamacher, "Decomposition and equilibrium achieving distribution locational marginal prices using trust-region method," *IEEE Trans. Smart Grid*, vol. 10, no. 3, pp. 3269–3281, May 2019.
[33] S. Hanif, P. Creutzburg, H. B. Gooi, and T. Hamacher, "Pricing mechanism for flexible loads using distribution grid hedging rights," *IEEE Trans. Power Syst.*, vol. 34, no. 5, pp. 4048–4059, Sep. 2019.
[34] A. K. Zarabie, S. Das, and M. N. Faqiry, "Fairness-regularized DLMP-based bilevel transactive energy mechanism in distribution systems," *IEEE Trans. Smart Grid*, vol. 10, no. 6, pp. 6029–6040, Nov. 2019.
[35] K. Zhang, S. Hanif, C. M. Hackl, and T. Hamacher, "A framework for multi-regional real-time pricing in distribution grids," *IEEE Trans. Smart Grid*, vol. 10, no. 6, pp. 6826–6838, Nov. 2019.
[36] M. B. Cain, R. P. O'Neill, and A. Castillo, "History of optimal power flow and formulations—Optimal power flow paper 1," Fed. Energy Regul. Com., Washington, DC, USA, Tech. Rep., 2012.
[37] J. Meisel, "System incremental cost calculations using the participation factor load-flow formulation," *IEEE Trans. Power Syst.*, vol. 8, no. 1, pp. 357–363, Feb. 1993.
[38] R. D. Zimmerman, C. E. Murillo-Sánchez, and R. J. Thomas, "MATPOWER: Steady-state operations, planning, and analysis tools for power systems research and education," *IEEE Trans. Power Syst.*, vol. 26, no. 1, pp. 12–19, Feb. 2011.
[39] O. Alsac and B. Stott, "Optimal load flow with steady-state security," *IEEE Trans. Power App. Syst.*, vol. PAS-93, no. 3, pp. 745–751, May 1974.
[40] K. Singh, N. P. Padhy, and J. Sharma, "Influence of price responsive demand shifting bidding on congestion and LMP in pool-based day-ahead electricity markets," *IEEE Trans. Power Syst.*, vol. 26, no. 2, pp. 886–896, May 2011.
[41] *PJM Manual 11: Energy & Ancillary Services Market Operations*, PJM, Norristown, PA, USA, 2022.

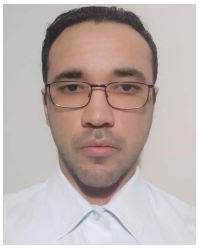

FELIPE O. S. SARAIVA (Member, IEEE) received the B.S., M.S., and Ph.D. degrees in electrical engineering from the Federal University of Maranhão (UFMA), São Luís, Brazil, in 2015, 2017, and 2021, respectively. He is currently a Postdoctoral Researcher with the Department of Electrical Engineering, UFMA. His research interests include electricity markets, power system operation and planning, and renewable energy integration.

V. LEONARDO PAUCAR (Senior Member, IEEE) received the B.S. and P.E. degrees in electrical engineering from the National University of the Center of Peru (UNCP), Peru, the M.S. degree in electrical engineering from the Pontificia Universidad Católica de Chile, Santiago, Chile, in 1989, and the Ph.D. degree in electrical engineering from the State University of Campinas (UNICAMP), Brazil, in 1998. He was a Professor with the Faculty of Electrical and Electronics Engineering, National University of Engineering (UNI), Lima, Peru. He is currently a Professor with the Department of Electrical Engineering, Federal University of Maranhão (UFMA), Brazil. His research interests include electricity markets, power system operation and control, and applications of artificial intelligence in electrical energy systems.